

# A METHOD OF ENHANCING SOURCE DETECTION SENSITIVITY IN GAUSSIAN NOISE, WITH APPLICATION TO PSR 1937+21 AND GW150914

RICHARD LIEU<sup>1</sup> AND KRISTEN A. LACKEOS<sup>2</sup>

<sup>1</sup>Department of Physics, University of Alabama, Huntsville, AL 35899  
 and

<sup>2</sup> NASA Postdoctoral Program Fellow, NASA Marshall Space Flight Center, Huntsville, AL 35812, USA

## ABSTRACT

The Gaussian phase noise of intensity time series is demonstrated to be drastically reduced when the raw voltage data are digitally filtered through an arbitrarily large number  $n$  of orthonormal bandpass profiles (eigen-filters) sharing the same intensity bandwidth, and the resulting intensity series are co-added. Specifically, the relative noise variance of the summed series at the resolution of one coherence time or less, goes down with increasing  $n$  as  $1/n$ , although (consistent with the radiometer equation) the advantage gradually disappears when the series is bin averaged to lower resolution. Thus the algorithm is designed to enhance the sensitivity of detecting transients that are smoothed out by time averaging and too faint to be visible in the noisy unaveraged time series, as demonstrated by the simulation of a weak embedded time varying signal of either a periodic nature or a fast and unrepeatable pulse. The algorithm is then applied to a 10 minute observation of the pulsar PSR 1937+21 by the VLA, where the theoretical predictions were verified by the data. Moreover, it is shown that microstructures within the time profile are better defined as the number  $n$  of filters used increases, and a periodic signal of period  $1.86 \times 10^{-5}$  s (53.9 kHz) is discovered in the pulse profile. Lastly, we apply the algorithm to the first binary black hole merger detected by LIGO, GW150914. We find the SNR of the mean peak intensity increases as  $\sqrt{n}$  and cross correlation of the event between the LIGO-Hanford-Livingston detector pair increases with filter order  $n$ .

## 1. INTRODUCTION

Communication in the radio differs from most other wavelengths of the electromagnetic spectrum in one key respect: the number of photons in some observed dataset is sufficiently large to consign the Poisson fluctuation in the arrival time of each photon (also called shot noise) to the realm of insignificance relative to another inevitable noise source, *viz.* Gaussian noise (also called photon bunching noise) which is a characteristic attribute of the wave nature of light. In quantitative terms, the relative importance of these two fundamental noise components in naturally occurring light is the photon occupation number  $n_0$ , which in the context of a time series of measured intensities is the number of arriving photons per unit frequency bandwidth  $\Delta\nu$  per unit coherence time  $\tau \approx 1/\Delta\nu$ .

The criterion on  $n_0$  is derived in many textbooks and review articles on the subject such as Loudon (2000). Explicitly, as we shall see below, for phase noise to be more important than shot noise the inequality

$$\frac{n_0 T}{\tau} \gg 1, \quad (1)$$

where  $T$  is the sampling time, must be satisfied. Physically it means the average number of photons arriving within a sampling interval is  $\gg 1$ . If there are  $N$  time contiguous samplings that comprise a total exposure of  $\mathcal{T} = NT \gg \tau$ , the ratio of square of the mean intensity to the noise power will for Gaussian chaotic light be of order the number of coherence time intervals within the total exposure, *viz.*  $\approx \mathcal{T}/\tau$ . This result is often referred to as the radiometer equation (Burke & Graham-Smith (2010); Christiansen & Högbom (1985)), and stems from the simple realization that in the intensity time series the noise fluctuation tends to randomly cancel among the various coherence segments but not within each of them. Another argument would interpret  $\mathcal{T}/\tau \approx \mathcal{T}\Delta\nu$  as the number of independent Fourier modes in the intensity time series, *i.e.* the accuracy of a mean intensity measurement over the interval  $\mathcal{T}$  is not controlled by the number  $N$  of sampling intervals  $T$  but the product of the two. Thus  $\mathcal{T}/\tau$  may also be interpreted as the minimum number of samples required to fully determine the characteristics of all the constituent modes – it is not necessary to sample the intensity (or voltages) more than the Nyquist limit of once per coherence time  $\tau$ . The radiometer equation

was recently shown by [Nair & Tsang \(2015\)](#) to be a fundamental unsurpassable limit on the uncertainty in the mean intensity of Gaussian noise dominated light over an exposure time  $\mathcal{T} \gg \tau$ .

The purpose of this paper is to demonstrate, both theoretically and with real data, that despite the limit imposed by the radiometer equation it is possible to process the time series of radio voltages to various degrees of sophistication to enhance the detection of transient signals embedded in Gaussian noise. We emphasize that our proposed methodology is not in conflict with the radiometer equation, nor does it produce a biased estimate of the mean intensity of Gaussian chaotic light. Rather, it merely lowers the noise variance from some original value  $\sigma_I^2$  to a smaller value  $\sigma_I'^2 < \sigma_I^2$ , by stretching the correlation length of the intensity time series. It shall be shown that the mean intensity over an interval  $\mathcal{T} \gg \tau$  is still governed by the radiometer equation, but an embedded source of duration  $\Delta t$  satisfying  $\Delta t \gtrsim \tau^1$  is detected more readily by the new approach.

The plan of the paper is to begin with a revisit of the basics of Gaussian noise, including a derivation of the radiometer equation. This will be followed by a mathematical treatment of the way our proposed methodology of noise suppression on the scale of  $\tau$  enhances the signal-to-noise of transient sources whilst maintaining consistency with the radiometer equation, and two simulations to test the theoretical predictions. We then apply the algorithm to a VLA observation of the millisecond pulsar PSR B1937+21 where it will be shown that, depending upon the number of iterations being used in the data processing stage, the pulsar light curve within a narrow band becomes increasingly better defined, and a hidden periodicity at higher harmonic number is revealed. The algorithm is lastly applied to LIGO event GW150914, the first gravitational wave observation, and the analysis is found to be in agreement theory.

## 2. TWO-POINT CORRELATION OF VOLTAGE AND INTENSITY OF STATIONARY GAUSSIAN LIGHT

Owing to the approximation of high occupation number,  $n_0 \gg 1$ , shot noise is negligible and one can calculate  $n$ -point amplitude correlations classically by treating the quantum operators as c-numbers, [Wang et al \(1989\)](#). For a Gaussian chaotic light (also known as Gaussian thermal light), such as especially radio noise, the voltage may be written as a linear superposition of Fourier amplitudes at random phase, *viz.*

$$V(t) = \sum_{j=1}^{N_m} a_j e^{i(\omega_j t + \phi_j)}, \quad (2)$$

where  $a_j = a(\omega_j)$ , the number of modes is  $N_m = \mathcal{T}\Delta\nu$  with  $\mathcal{T}$  being the total exposure time and  $\Delta\nu$  the bandwidth, and the phases  $\phi_j$  are random and uncorrelated.

The time series of  $V(t)$  is evidently governed by a stationary stochastic process with vanishing ensemble mean,  $\langle V(t) \rangle = 0$ . The two point function of  $V(t)$  is

$$\langle V(t)V^*(t+t') \rangle = \left\langle \sum_j a_j e^{i(\omega_j t + \phi_j)} \sum_k a_k^* e^{-i[\omega_k(t+t') + \phi_k]} \right\rangle, \quad (3)$$

where the range of the summation for  $j$  and  $k$  are now dropped, with the understanding that it is from 1 to  $N_m$  for both. The ensemble average of the two point function,  $\langle V(t)V^*(t+t') \rangle$  is obtained by noting that in ((3)) unless  $j = k$  this average vanishes. Thus the result is independent of  $t$ , and (moreover) one may replace  $t'$  by  $t$  by writing

$$\langle V(0)V^*(t) \rangle = \sum_j |a_j|^2 e^{-i\omega_j t}. \quad (4)$$

In the continuum limit this becomes the Fourier transform of the amplitude  $a(\omega)$ , *i.e.* if  $a(\omega)$  is centered at  $\omega = \omega_0$  and spans the bandwidth  $\Delta\omega = 2\pi\Delta\nu$ ,  $\langle V(0)V^*(t) \rangle$  would typically be finite over some time interval of size  $\tau \approx 1/\Delta\nu$ , which may be taken as the coherence length of the voltage autocorrelation function.

At zero lag  $t = 0$ ,  $\langle V(0)V^*(t) \rangle$  becomes the mean intensity of the beam. The intensity two-point function is

$$\begin{aligned} I(t)I(t+t') &= V(t)V^*(t)V(t+t')V^*(t+t') \\ &= \sum_j a_j e^{i(\omega_j t + \phi_j)} \sum_k a_k^* e^{-i(\omega_k t + \phi_k)} \sum_p a_p e^{i[\omega_p(t+t') + \phi_p]} \sum_q a_q^* e^{-i[\omega_q(t+t') + \phi_q]}. \end{aligned} \quad (5)$$

As before, due to the random phases the ensemble average  $I(t)I(t+t')$  is obtained by noting the only two combinations of summation indices that yield finite contributions, *viz.*  $j = k$ ,  $p = q$  and  $j = q$ ,  $k = p$ . Thus again, independently of

<sup>1</sup> The fastest transient allowed by the Fourier bandwidth theorem is  $\Delta t \approx \tau$

$t$  so that one can set  $t = 0$  and rewrite  $t'$  as  $t$ ,

$$\begin{aligned} \langle I(0)I(t) \rangle - \langle I \rangle^2 &= \langle V(0)V^*(0)V(t)V^*(t) \rangle - \langle V(0)V^*(0) \rangle^2 \\ &= \left| \sum_j a_j a_j^* e^{-i\omega_j t} \right|^2. \end{aligned} \quad (6)$$

Thus in the continuum limit the intensity covariance function is the modulus square of the Fourier transform of  $|a(\omega)|^2$ . If, as in the case of the voltage correlation,  $a(\omega)$  spans the bandwidth  $\Delta\omega$ , the intensity covariance function will extend to the coherence length  $\tau$  which is the reciprocal of the bandwidth.

To be very precise about the relationship between coherence length and bandwidth, let the spectrum of an arriving radiation beam be of the form

$$|a(\omega)|^2 = \frac{n_0}{\sqrt{2\pi}\mathcal{T}} e^{-(\omega-\omega_0)^2 \tau^2/2}. \quad (7)$$

This spectrum may be intrinsic to the source itself, or due to a bandpass filter being physically or digitally applied to an otherwise spectrally flat source. Then the summation in ((6)), when evaluated as an integral, becomes

$$\langle I(0)I(t) \rangle - \langle I \rangle^2 = \left| \mathcal{T} \int_{-\infty}^{\infty} |a(\omega)|^2 e^{-i\omega t} d\omega \right|^2 = \frac{n_0^2}{\tau^2} e^{-t^2/\tau^2}. \quad (8)$$

Since, from ((4)), the mean intensity is  $\langle V(0)V^*(0) \rangle = n_0/\tau$ , ((8)) yields the normalized covariance function (autocorrelation function, ACF)

$$\frac{\langle I(0)I(t) \rangle - \langle I \rangle^2}{\langle I \rangle^2} = e^{-t^2/\tau^2}, \quad (9)$$

from which one reads off the relative variance of the intensity as

$$\frac{\sigma_I^2}{\bar{I}^2} = \frac{\langle I(0)I(0) \rangle - \langle I \rangle^2}{\langle I \rangle^2} = 1. \quad (10)$$

Note that ((10)) is a fundamental property of Gaussian noise, *viz.* the variance equals the square of the mean intensity. More generally, for any spectrum  $|a(\omega)|^2$ , ((9)) may be written as

$$\frac{\langle I(0)I(t) \rangle - \langle I \rangle^2}{\langle I \rangle^2} = |f(t)|^2, \quad (11)$$

where

$$f(t) = \frac{\int_{-\infty}^{\infty} |a(\omega)|^2 e^{-i\omega t} d\omega}{\int_{-\infty}^{\infty} |a(\omega)|^2 d\omega}. \quad (12)$$

is a complex function satisfying  $f(t) = 1$  at  $t = 0$  while having finite values in the range  $|t| \lesssim \tau \approx 1/\Delta\nu$ . Also from ((7)) and the relation  $\mathcal{T}\delta\nu = 1$  where  $\delta\nu$  is the mode spacing,

$$\mathcal{T} \int_{-\infty}^{\infty} \frac{1}{2\pi} |a(\omega)|^2 d\omega = \sum_j |a(\omega_j)|^2 = \frac{n_0}{\tau}, \quad (13)$$

is the ensemble mean intensity (or flux).

Let us next examine what happens when the intensity measured over some small but finite interval  $T \ll \tau$ . The result may be expressed as

$$I_r = \frac{1}{T} \int_{t_r-T}^{t_r} dt' I(t'). \quad (14)$$

The normalized covariance between two intensity measurements which took place during intervals  $T$  centered at times  $t_r$  and  $t_s$  is, from ((11)),

$$\frac{\text{cov}(I_r, I_s)}{\langle I \rangle^2} = |f_{rs}|^2, \quad (15)$$

where

$$|f_{rs}|^2 = |f(t_r - t_s)|^2 = |f((r-s)T)|^2 \quad (16)$$

also has the properties  $|f_{rs}|^2 = 1$  for  $r = s$  and  $|f_{rs}|^2 = 0$  for  $|t_r - t_s| \gg \tau$ .

Turning to the variance of these measurements, it is given by

$$\frac{\text{var}(I_r)}{\langle I \rangle^2} = \frac{\text{cov}(I_r, I_s)}{\langle I \rangle^2} = 1. \quad (17)$$

But what if many of these small samples are time contiguously averaged to form the mean intensity

$$I_{\mathcal{T}} = \frac{1}{N} \sum_{r=1}^N I_r \quad (18)$$

over the much longer interval  $\mathcal{T} = NT \gg \tau$  (because  $N \gg 1$ )? In this case the variance of  $I_{\mathcal{T}}$  is

$$\text{var}(I_{\mathcal{T}}) = \frac{1}{N^2} \sum_{r,s=1}^N \text{cov}(I_r, I_s). \quad (19)$$

When we substitute from ((15)), we can convert the sum over  $u = r - s$  to the Gaussian integral

$$\sum_u |f(uT)|^2 \approx \frac{1}{T} \int dt |f(t)|^2 \approx \frac{\tau}{T}, \quad (20)$$

while the other one of the double sum becomes  $N$ . In this way we obtain

$$\frac{\text{var}(I_{\mathcal{T}})}{\langle I \rangle^2} \approx \frac{\tau}{NT} = \frac{\tau}{\mathcal{T}}, \quad (21)$$

which is the radiometer equation. For the Gaussian spectrum of ((7)) where  $|f(t)|^2$  is given by  $\exp(-t^2/\tau^2)$ , the right side ((21)) assumes the more precise expression  $\sqrt{\pi}\tau/\mathcal{T}$ .

It is also possible to directly calculate the variance of an intensity sample averaged over *any* duration  $\mathcal{T}$  as

$$\text{var}(I_{\mathcal{T}}) = \frac{n_0^2}{\tau \mathcal{T}} F\left(\frac{\mathcal{T}}{\tau}\right), \quad (22)$$

where

$$F\left(\frac{\mathcal{T}}{\tau}\right) = \frac{1}{\tau \mathcal{T}} \int_{-\mathcal{T}}^{\mathcal{T}} dt (\mathcal{T} - |t|) |f(t)|^2 \quad (23)$$

with  $f(t)$  being defined in ((11)). If  $\mathcal{T}$  is short compared to the coherence time  $\tau$ ,  $|f(t)|^2 \approx 1$  and ((23)) reduces to  $F(\mathcal{T}/\tau) \approx \mathcal{T}/\tau$ . Since the ensemble mean intensity is  $n_0/\tau$  from ((13)), we arrive once again at ((17)), *viz.* a relative intensity variance of unity. On the other hand, if  $\mathcal{T} \gg \tau$ , we must then use the limiting value of  $F(x) \approx 1$  for  $x \gg 1$  to arrive at  $\tau/\mathcal{T}$  as the approximate expression of the relative variance; for the Gaussian spectrum with  $|f(t)|^2 = \exp(-t^2/\tau^2)$ , this becomes  $\sqrt{\pi}\tau/\mathcal{T}$  as before.

### 3. GAUSSIAN NOISE SUPPRESSION ON SHORT TIMESCALES BY DIGITAL FILTERING

Let there be a raw data set consisting of real voltages  $V_r$  measured over times  $t_r$  where  $1 \leq r \leq N$ ,  $t_{r+1} - t_r = T$ , and  $NT = \mathcal{T}$  as before. Let the data be sampled at the Nyquist rate, *viz.*  $T$  is of order the coherence time. Now suppose  $V_r$  is frequency filtered *digitally* into a much narrower bandwidth (equivalently the time series is convolved with a wide kernel) centered at the same  $\omega_0 = 2\pi\nu_0$  as the original mid-band frequency and with  $\alpha_r$  being the resulting oversampled voltages – oversampled because now  $T$  is much less than the coherence time of the Gaussian noise fluctuations. Suppose further that the exercise is repeated using a different filter which is also centered at  $\omega_0$  and much narrower than the original bandwidth, leading to the voltage series  $\beta_s$  with  $1 \leq s \leq N$ .

We assume for simplicity that the raw spectrum is essentially flat between its lower and upper frequency limits, and the two narrow filtered intensity spectrum  $|a_j|^2$  and  $|b_k|^2$  (with  $1 \leq j \leq N_m \approx \mathcal{T}\Delta\nu$  and likewise for the index  $k$ ) share the same bandwidth  $\Delta\nu$ , *i.e.* the filters only differ by their shapes in amplitude space  $a_j$  and  $b_k$ . Thus the two intensity time series  $I_r = |\alpha_r|^2$  and  $I'_r = |\beta_r|^2$  not only span the same time interval  $\mathcal{T}$ , but also share the same radiation frequencies. We shall illustrate these abstract notions with a concrete example below. Following the arguments of the previous section,  $I_r$  and  $I'_r$  have ensemble intensities

$$\langle I \rangle = \sum_j |a_j|^2; \text{ and } \langle I' \rangle = \sum_k |b_k|^2. \quad (24)$$

The relative variance for  $I_r$  is

$$\frac{\sigma_I^2}{\bar{I}^2} = \frac{\langle I^2 \rangle - \langle I \rangle^2}{\langle I \rangle^2} = 1, \quad (25)$$

and the equation also holds for  $I'_r$ .

We now turn to the series  $\mathcal{I}_r = I_r + I'_r$  which has the ensemble mean of

$$\langle \mathcal{I} \rangle = \sum_j (|a_j|^2 + |b_j|^2) = \langle I \rangle + \langle I' \rangle, \quad (26)$$

and variance

$$\langle \mathcal{I}^2 \rangle - \langle \mathcal{I} \rangle^2 = \langle I \rangle^2 + \langle I' \rangle^2 + 2(\langle II' \rangle - \langle I \rangle \langle I' \rangle). \quad (27)$$

Of interest here are the last two terms, to be analyzed next.

Starting with

$$\begin{aligned} I(t)I'(t+t') &= V(t)V'^*(t)V(t+t')V'^*(t+t') \\ &= \sum_j a_j e^{i(\omega_j t + \phi_j)} \sum_k a_k^* e^{-i(\omega_k t + \phi_k)} \sum_p b_p e^{i[\omega_p(t+t') + \phi_p]} \sum_q b_q^* e^{-i[\omega_q(t+t') + \phi_q]}, \end{aligned} \quad (28)$$

one sees that when computing the ensemble average of  $I(t)I'(t+t')$  at  $t' = 0$  the  $j = k$  and  $p = q$  pairings yield  $\langle I \rangle \langle I' \rangle$ , while the  $j = q$  and  $k = p$  pairings yield  $|\sum_j a_j b_j^*|^2$  which satisfies the Schwarz inequality

$$\left| \sum_j a_j b_j^* \right|^2 < \sum_j |a_j|^2 \sum_k |b_k|^2 = \langle I \rangle \langle I' \rangle, \quad (29)$$

and the  $<$  sign is always valid provided  $a_j$  and  $b_k$  are linearly independent sequences. In this case, ((27)) and ((28)) imply

$$\frac{\text{var}(\mathcal{I}_r)}{\langle \mathcal{I} \rangle^2} < 1, \quad (30)$$

where  $\text{var}(\mathcal{I}_r) = \sigma_{\mathcal{I}}^2 = \langle \mathcal{I}^2 \rangle - \langle \mathcal{I} \rangle^2$ .

Thus, we constructed a time series with an unbiased estimate of the mean (in the sense that the arithmetic mean of  $\mathcal{I}_r$  tends to the ensemble mean  $\langle \mathcal{I} \rangle$  as the sample size tends to infinity), but with *less* relative variance than the standard Gaussian noise of ((17)). Under the particular scenario of

$$\sum_j |a_j|^2 = \sum_j |b_j|^2; \text{ and } \sum_j a_j b_j^* = 0, \quad (31)$$

the relative variance of ((30)) has 0.5 as its expectation value, which is half the standard value of ((17)). Moreover, the technique may readily be extended to accommodate more than two digital filters. Thus, for three filters satisfying

$$\sum_j |a_j|^2 = \sum_j |b_j|^2 = \sum_j |c_j|^2; \text{ and } \sum_j a_j b_j^* = 0, \sum_j a_j c_j^* = 0, \sum_j b_j c_j^* = 0 \quad (32)$$

the relative variance of  $\mathcal{I}_r = I_r + I'_r + I''_r$  has the expectation value of  $1/3$ . And it is also not difficult to prove the general result for  $n$  filters is a relative variance of  $1/n$ , which can be negligibly small for arbitrarily large  $n$  whilst maintaining the status of sample mean of  $\mathcal{I}$  as an unbiased  $\langle I \rangle$  estimator. In Figure 1 we illustrate the design of a set of 6 filters (*i.e.* up to  $n = 6$ , or ‘6-part’).

Can two filters be digitally designed to satisfy ((31)) for any incident radiation having a flat spectrum within the (narrow) bandpass, where each radiation mode is taken to be of unit strength? Assuming the filter amplitudes  $a_j$  are real and positive numbers distributed symmetrically about the band center  $\nu_j = \nu_0$ , one viable option is to digitally set  $b_j = a_j$  for  $\nu_j < \nu_0$  and  $b_j = -a_j$  for  $\nu_j \geq \nu_0$ , with  $a_j$  being a real number.

As a concrete example, consider the digital filters

$$a_j = e^{-(\omega_j - \omega_0)^2 \tau^2 / 4} \text{ for all } \omega_j; \quad b_j = \pm e^{-(\omega_j - \omega_0)^2 \tau^2 / 4} \text{ for } \omega_j \lessgtr \omega_0. \quad (33)$$

By observing from ((27)) that

$$\langle \mathcal{I}_r \mathcal{I}_s \rangle - \langle \mathcal{I} \rangle^2 = \left| \sum_j a_j a_j^* e^{-i\omega_j T(r-s)} \right|^2 + \left| \sum_j b_j b_j^* e^{-i\omega_j T(r-s)} \right|^2 + 2 \left| \sum_j a_j b_j^* e^{-i\omega_j T(r-s)} \right|^2, \quad (34)$$

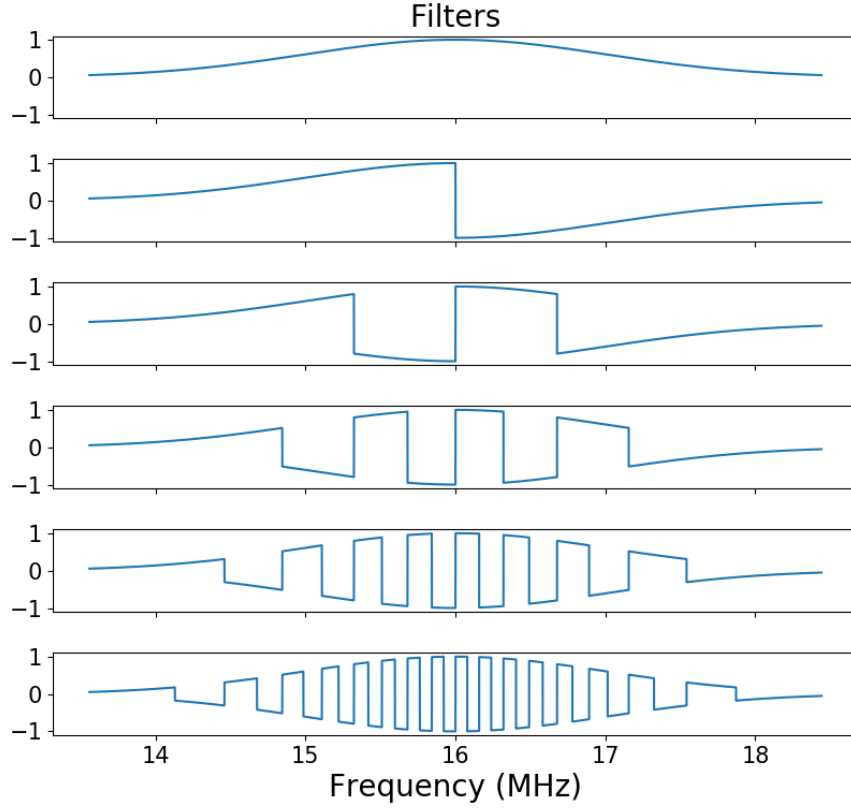


**Figure 1.** The 6-part combination of digital amplitude filters to reduce the relative variance of Gaussian radio noise by 6 times. All the structures share equal underlying areas (absolute values); and the square of each filter equals the square of the Gaussian filter at the top *i.e.* the intensity bandpass of the filters are the same.

and following the steps outlined after ((28)), one obtains

$$\frac{\text{cov}(\mathcal{I}_r, \mathcal{I}_s)}{\langle \mathcal{I} \rangle^2} = \frac{\langle \mathcal{I}_r \mathcal{I}_s \rangle - \langle \mathcal{I} \rangle^2}{\langle \mathcal{I} \rangle^2} = \frac{1}{2} e^{-(r-s)^2 T^2 / \tau^2} \left\{ 1 + \left[ \text{erfi} \left( \frac{(r-s)T}{\sqrt{2}\tau} \right) \right]^2 \right\} \approx \frac{1}{2} e^{-(r-s)^2 T^2 / (4\tau^2)} \quad (35)$$

By putting  $r = s$  to form the variance of  $\mathcal{I}_r$ , one readily deduces

$$\frac{\sigma_{\mathcal{I}}^2}{\langle \mathcal{I} \rangle^2} = \frac{\text{var}(\mathcal{I}_r)}{\langle \mathcal{I} \rangle^2} = \frac{1}{2} \quad (36)$$

since  $\text{erfi}(0) = 0$ . This is consistent with the specific manifestation of ((30)) in the appropriate limit of ((31)), and indicates that the  $\mathcal{I}_r$  time series has less Gaussian noise on short time scales.

When evaluating the variance of the sample average of  $\mathcal{I}_r$  over a much longer time scale such as  $\mathcal{T} = NT \gg \tau$ , however, one must apply ((35)) to ((19)). The result is still the radiometer equation ((21)), which confirms the claim of Nair & Tsang (2015) that the sensitivity limit imposed by this equation cannot be surpassed. To see how enforcement of ((21)) is brought about in detail, observe that although the erfi function in ((35)) vanishes at zero lag  $t = 0$ , it rises to a peak of order unity at  $t \approx \tau$  before decaying away. Consequently the intensity two point function in ((35)) has a height of 0.5 but a width  $\approx 2\tau$ , to be compared to the height of unity and width  $\approx \tau$  for  $\mathcal{I}_r$ . Thus the *area* under the two point function, which gives the relative variance of flux averages over time intervals  $\gg \tau$ , is in fact the same for both  $\mathcal{I}_{\mathcal{T}}$  and  $\mathcal{I}_r$ . The proof of this conclusion is extended in the Appendix to the case involving any pair of filters  $\{a_j\}$  and  $\{b_j\}$ . More generally, if  $n$  filters are employed, the relative variance of  $\mathcal{I}_r$  will be reduced to  $1/n$

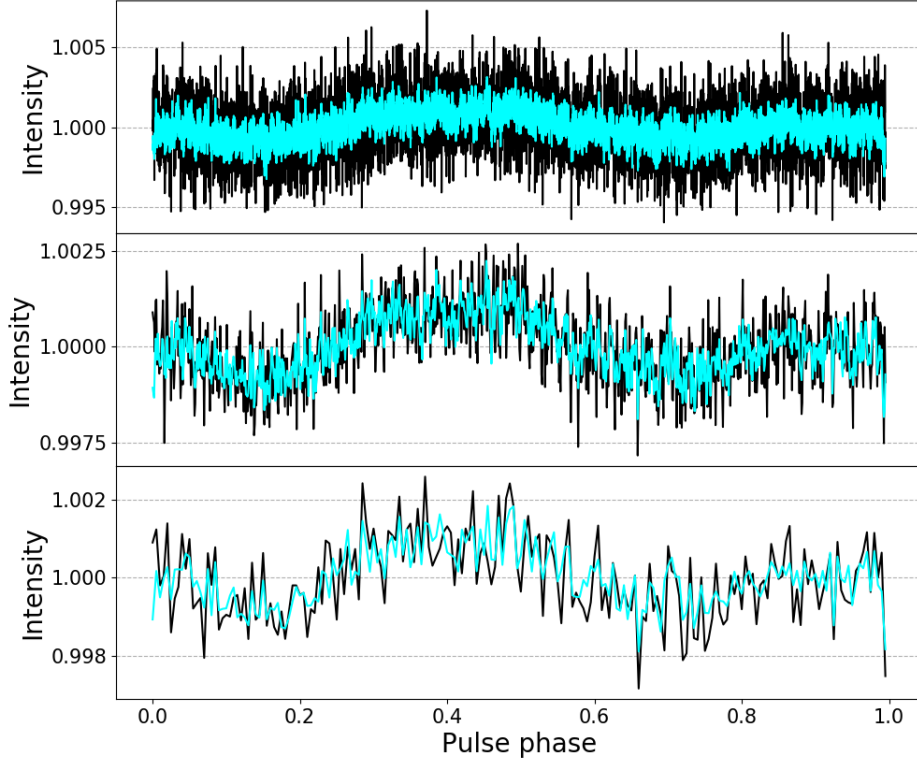


**Figure 2.** The pulse profile of the entire 10 minute VLA observation of PSR 1937+21, as obtained by folding the intensity time series modulo the pulse period. Note the considerably higher signal-to-noise of the 6-part time series relative to the conventional 1-part, when the full time resolution is applied. The advantage goes away with averaging over larger time bins.

as already explained, but the width of the covariance will be increased to  $\approx n\tau$ . Thus the area under the covariance curve remains unchanged w.r.t. to its value for  $I_r$ , and so the relative variance of  $\mathcal{I}_\tau$  is still given by the radiometer equation. Such behavior is quantitatively shown in Table 1 and Figure 2 in respect of processing a real observational data set, about which a graph of the two point function of  $I_r$  and  $\mathcal{I}_\tau$  is to be found in Figure 3.

Order of processing	$\text{var}(\mathcal{I}_\tau)/\langle I \rangle^2$ $\mathcal{T} = T$	$\text{var}(\mathcal{I}_\tau)/\langle I \rangle^2$ $\mathcal{T} = 100T$	$\text{var}(\mathcal{I}_\tau)/\langle I \rangle^2$ $\mathcal{T} = 500T$
1-part	0.99	0.24	0.052
2-part	0.50	0.20	0.049
3-part	0.36	0.18	0.047
4-part	0.27	0.14	0.044
5-part	0.21	0.11	0.040
6-part	0.17	0.08	0.03

**Table 1.** The signal-to-noise ratio of time series processed by filter combinations of increasing complexity, followed by bin averaging. Note the advantage of using an  $n$ -part filter combination with large  $n$  disappears when one performs long time averaging. Thus the methodology is only useful for the detection of transient signals that require high time resolution (hence a small averaging window  $\mathcal{T}$ ).

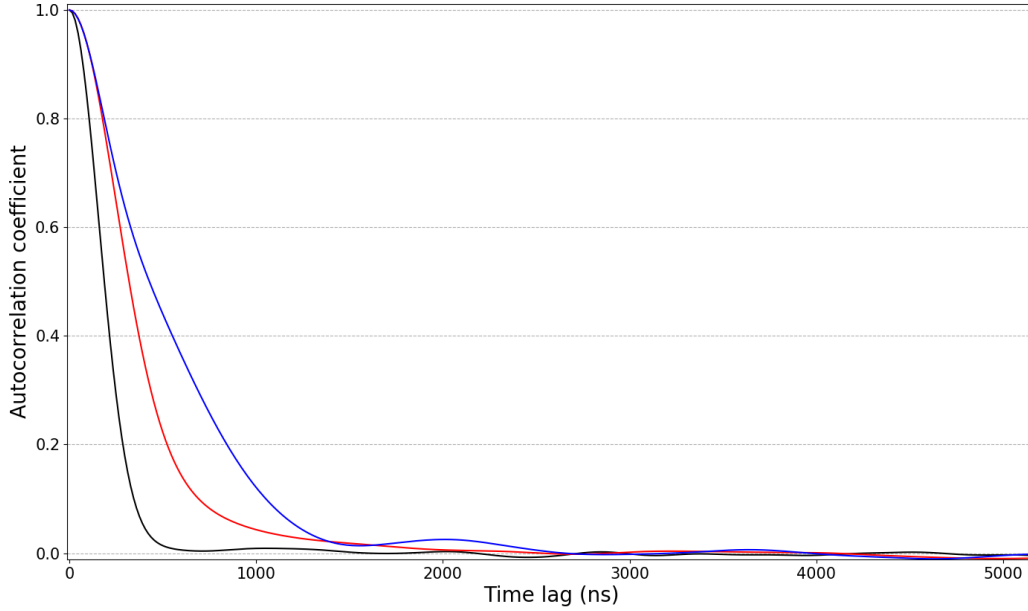


**Figure 3.** Autocorrelation function (ACF) of the intensity time series of various filter combinations. Each tick-mark of time lag is  $T = 15.626$  ns. The  $n$ -part ACF is wider than the 1-part by the factor  $n$ , and is roughly represented by a Gaussian form  $\exp[-t^2/(n^2\tau^2)]$ . The ACFs of 1-part through 3-part are shown here, with 1-part having the smallest correlation length and 3-part the largest.

#### 4. SIGNAL-TO-NOISE ENHANCEMENT OF TIME VARIABLE SOURCES

The interesting question arises, nonetheless, on what happens when a weak transient Gaussian noise source lasting a duration  $\gtrsim \tau$  is embedded in the time series. In general, one lets the amplitude of the source be enveloped by some function  $\epsilon(t)$  which is centered at  $t = t_0$  and of width  $\gtrsim \tau$ . The bandwidth of frequencies generated by such an envelope is obviously within the range spanned by  $\{a_j\}$  and  $\{b_k\}$  (*i.e.* the function  $\epsilon(t) e^{i\omega t}$  need not be resolved into modes for the analysis below). The intensity  $I(t)$  becomes

$$I(t) = V(t)V^*(t) = \sum_j a_j \left[ e^{i(\omega_j t + \phi_j)} + \epsilon(t) e^{i(\omega_j t + \varphi_j)} \right] \sum_k a_k^* \left[ e^{-i(\omega_k t + \phi_k)} + \epsilon^*(t) e^{-i(\omega_k t + \varphi_k)} \right], \quad (37)$$

with a similar expression for  $I'(t)$ . The ensemble averages are

$$\langle I(t) \rangle = \sum_j |a_j|^2 [1 + |\epsilon(t)|^2]; \quad \langle I'(t) \rangle = \sum_k |b_k|^2 [1 + |\epsilon(t)|^2], \quad (38)$$

and exhibit a small excess at around  $t = t_0$ . Repeating the calculation of the intensity autocorrelation in the same manner as ((28)), noting that the two sets of random phases  $\{\phi_j\}$  and  $\{\varphi_k\}$  are independent sets, we find as before  $\text{var}(I_r)/\langle I \rangle^2 = \text{var}(I'_r)/\langle I' \rangle^2 = 1$  to order  $\epsilon^2$ , with  $I_r$  as defined in ((14)) and  $\langle I \rangle$  and  $\langle I' \rangle$  as given by ((38)), but  $\text{var}(\mathcal{I}_r)/\langle \mathcal{I} \rangle^2 < 1$ . In the special choice of filters as prescribed by ((31)), the limit of 50 % noise reduction, *viz.* ((36)), is once again attained. Since the ensemble average is  $\langle \mathcal{I}_r \rangle = \langle \mathcal{I}(t_r) \rangle = \langle I(t_r) \rangle + \langle I'(t_r) \rangle$  for any choice of filters, where  $\langle I(t) \rangle$  and  $\langle I'(t) \rangle$  are once again as in ((38)), one sees that the noise is reduced without compromising any signal strength.

The key advantage in terms of source detection, however, is that for a transient source one does not detect it by measuring and computing the average intensity over some long duration  $\mathcal{T} \gg \tau$  (when the noise-to-signal ratio has returned (*i.e.* deteriorated back) to the limit given by the conventional radiometer equation); rather, one must enlist the full timing resolution of the observation. More precisely, a short segment of the time series of duration  $\gtrsim \tau$  is optimal to the search for such transients, and because the noise is significantly reduced w.r.t the signal over the time span of  $2\tau$ , this offers a means of finding burst sources more sensitively without resorting to a narrower band filter to



increase the coherence time  $\tau$ . If more than two filters sharing the same intensity bandwidth (as the original single filter scenario) are used in accordance with the prescription of ((32)) and what followed, one would be able to look for a broader class of transients lasting the duration  $\Delta t \lesssim n\tau$  where  $n$  is the number of filters used, with a reduction of the relative variance by the factor of  $n$ . The source strength, on the other hand, stays the same, so that the sensitivity of source detection is then enhanced by the factor  $\sqrt{n}$ .

#### 4.1. A periodic embedded signal

To formulate the above in more precise terms, we consider the specific scenario of a chaotic light source with a flat spectrum (in some relevant frequency range) and emitting periodically. The voltage at the receiver is given by

$$\epsilon(t) = \epsilon_0 \sin \Omega t \sum_j e^{i(\omega_j t + \varphi_j)}. \quad (39)$$

Let the signal be embedded in a likewise spectrally flat background noise, so that the observed voltage at time  $t$  has the normalized form

$$\mathcal{V}(t) = \epsilon(t) + \sum_k e^{i(\omega_k t + \phi_k)}. \quad (40)$$

Upon Fourier transforming to the frequency domain, one obtains

$$\tilde{\mathcal{V}}(\omega) = \frac{\pi \epsilon_0}{i} \sum_j e^{i\varphi_j} [\delta(\omega_j + \Omega - \omega) - \delta(\omega_j - \Omega - \omega)] + 2\pi \sum_k e^{i\phi_k} \delta(\omega_k - \omega), \quad (41)$$

where  $\epsilon_0 \ll 1$  and the phases  $\{\varphi_j\}$  and  $\{\phi_k\}$  are uncorrelated.

After applying a narrow band filter  $\{\mathbf{a}\}$  to select a smaller range of frequencies, the voltage spectral amplitude becomes

$$\tilde{V}(\omega) = \frac{\pi \epsilon_0}{i} \sum_j a_j e^{i\varphi_j} [\delta(\omega_j + \Omega - \omega) - \delta(\omega_j - \Omega - \omega)] + 2\pi \sum_k a_k e^{i\phi_k} \delta(\omega_k - \omega), \quad (42)$$

Inversion back to the time domain yields

$$V(t) = \frac{\epsilon_0}{2i} \sum_j e^{i(\omega_j t + \varphi_j)} [a(\omega_j + \Omega) e^{i\Omega t} - a(\omega_j - \Omega) e^{-i\Omega t}] + \sum_k a_k e^{i(\omega_k t + \phi_k)} \quad (43)$$

Provided  $\Omega \ll \omega_j$  for all  $\omega_j$  within the selected band, one may assume  $a(\omega_j + \Omega) \approx a(\omega_j - \Omega) \approx a(\omega_j) = a_j$  (or equivalently  $\Omega$  is a small fraction of the filter bandwidth  $\Delta\omega$ ), in which case ((43)) simplifies to

$$V(t) = \epsilon_0 \sin \Omega t \sum_j a_j e^{i(\omega_j t + \varphi_j)} + \sum_k a_k e^{i(\omega_k t + \phi_k)} \quad (44)$$

This is the voltage time series an observer measures.

From ((44)) we proceed to calculate the mean intensity of the beam in a manner analogous to ((3)) as the voltage two-point function at zero lag, *viz.*

$$\langle I(t) \rangle = (1 + \epsilon_0^2 \sin^2 \Omega t) \sum_j a_j^2. \quad (45)$$

The intensity two-point function is

$$\langle I(t)I(t+\tau) \rangle - \langle I(t) \rangle \langle I(t+\tau) \rangle = \left| \sum_j a_j^2 e^{-i\omega_j \tau} \right|^2 [1 + \epsilon_0^4 \sin^2 \Omega t \sin^2 \Omega(t+\tau)] \approx \left| \sum_j a_j^2 e^{-i\omega_j \tau} \right|^2, \quad (46)$$

where the approximation sign means one discarded a term of order  $\epsilon_0^4 \lll 1$  (or the square of the ratio of the signal intensity to the background intensity) relative to the term kept. This indicates that the variance is much more dominated by the background noise than the mean intensity.

#### 4.2. Detection sensitivity

For two beams ensuing from orthonormal filters  $\{\mathbf{a}\}$  and  $\{\mathbf{b}\}$  satisfying ((31)), the intensity two-point function yields

$$\langle I_1(t)I_2(t+\tau) \rangle - \langle I_1(t) \rangle \langle I_2(t+\tau) \rangle = \left| \sum_j a_j b_j e^{-i\omega_j \tau} \right|^2 [1 + \epsilon_0^4 \sin^2 \Omega t \sin^2 \Omega(t+\tau)] \approx \left| \sum_j a_j b_j e^{-i\omega_j \tau} \right|^2 \quad (47)$$

and vanishes exactly when  $\tau = 0$ . Thus, when the two beams are combined to form the total intensity  $\mathcal{I} = I_1 + I_2$ , the signal of interest is manifested as an intensity difference (modulation) between two times  $t_r$  and  $t_s$ , *viz.*

$$\langle \mathcal{I}_r - \mathcal{I}_s \rangle = 2\epsilon_0^2 \mathbf{a} \cdot \mathbf{a} (\sin^2 \Omega t_r - \sin^2 \Omega t_s), \quad (48)$$

where it is assumed that  $\mathbf{a} \cdot \mathbf{a} = \mathbf{b} \cdot \mathbf{b}$  in accordance with the normalizing condition of the filters as given by the first part of ((31)). The noise variance, on the other hand, is (by ((47)) with  $\tau = 0$ )  $\langle \mathcal{I}^2 \rangle - \langle \mathcal{I} \rangle^2 = 2(\mathbf{a} \cdot \mathbf{a})^2$  if  $|t_r - t_s| \gg 2/\Delta\omega$  (or  $n/\Delta\omega$  in the case of  $n$  orthonormal filters), and  $\langle \mathcal{I}^2 \rangle - \langle \mathcal{I} \rangle^2 \approx 0$  if  $|t_r - t_s|$  is otherwise. Thus the signal-to-noise ratio is  $\sqrt{2}\epsilon_0^2\eta$  where  $\eta = \sin^2 \Omega t_r - \sin^2 \Omega t_s$ , or  $2\epsilon_0^4\eta^2$  if expressed as the square of the signal intensity divided by the noise variance (as is the case when one estimates the signal significance in terms of the power spectral density at frequency  $2\Omega$ ). Likewise, it can readily be shown that if only one beam  $I_1$  (or  $I_2$ ) is employed the corresponding signal-to-noise ratios are  $\epsilon_0^2\eta$  (or  $\epsilon_0^4\eta^2$ ) but if the intensity of  $n$  orthogonally filtered beams are added they become  $n\epsilon_0^2\eta/\sqrt{n}$  (or  $n\epsilon_0^4\eta^2$ ). In this way the advantage of using multiple beams is indicated.

It should also be emphasized that although on one hand the proposed technique works optimally when  $\Omega$  is much smaller than the filter bandwidth  $\Delta\omega = 2\pi\Delta\nu$  as explained after ((43)), one does not require  $n\Omega$  to satisfy the same criterion. In fact, if  $n$  orthogonally filtered beams are enlisted the optimal frequency  $\Omega$  of the embedded signal is

$$\Omega \ll \Delta\omega \text{ but } n\Omega \gtrsim \Delta\omega. \quad (49)$$

This is because when  $n\Omega < \Delta\omega$  one can average the intensity data over  $n$  coherence lengths (*i.e.* the timescale  $n/\Delta\omega$ ) without smoothing out the signal oscillation, in which case the relative variance of the summed intensity of the  $n$  beams approaches the single beam scenario as noted in section 3, and the signal-to-noise advantage of the former over the latter is no longer remarkable. The overall message is that for a small value of  $\Omega$ , more orthogonally filtered beams have to be combined to achieve significant detection sensitivity of the oscillating signal.

#### 4.3. Power spectrum of intensity variation

To further elaborate upon the above analysis, we calculate the power spectrum of intensity fluctuation, *i.e.* the modulus square of the Fourier transform of the intensity time series, which has the expectation value

$$\langle |\tilde{\mathcal{I}}(\omega)|^2 \rangle = \int_{-\mathcal{T}/2}^{\mathcal{T}/2} dt_2 \int_{-\mathcal{T}/2}^{\mathcal{T}/2} dt_1 e^{i\omega(t_2-t_1)} \langle \mathcal{I}(t_1)\mathcal{I}(t_2) \rangle. \quad (50)$$

Now as long the phases  $\{\varphi_j\}$  and  $\{\phi_j\}$  in ((41)) are uncorrelated, use can be made of equations like ((46)) and ((47)) to deduce that

$$\begin{aligned} \langle \mathcal{I}(t_1)\mathcal{I}(t_2) \rangle &= \langle \mathcal{I}_b \rangle^2 (1 + \epsilon_0^2 \sin^2 \Omega t_1 + \epsilon_0^2 \sin^2 \Omega t_2 + \epsilon_0^4 \sin^2 \Omega t_1 \sin^2 \Omega t_2) \\ &\quad + \xi(t_2 - t_1)(\epsilon_0^4 \sin^2 \Omega t_1 \sin^2 \Omega t_2 + 1), \end{aligned} \quad (51)$$

where

$$\xi(t) = \langle I_b(0)I_b(t) \rangle - \langle I_b \rangle^2, \quad (52)$$

is the two-point function of the background intensity (*i.e.* intensity  $I_b$  in the absence of the periodic signal).

When ((51)) is substituted into ((50)), the first three terms on the right side of ((51)) contribute nothing to the signal power  $\langle |\tilde{\mathcal{I}}(\omega)|^2 \rangle$  in the vicinity of  $\omega = 2\Omega$ , while the next three terms yield respectively the ones on the right side of the following equation

$$\langle |\tilde{\mathcal{I}}(\omega)|^2 \rangle = \langle \mathcal{I}_b \rangle^2 \left[ \frac{\pi^2 \epsilon_0^4}{16} \delta^2(\omega - 2\Omega) + \frac{\sqrt{\pi} \epsilon_0^4 \mathcal{T} \tau}{16} e^{-n^2 \tau^2 (\omega - 2\Omega)^2 / 4} + \sqrt{\pi} \mathcal{T} \tau e^{-n^2 \tau^2 \omega^2 / 4} \right], \quad (53)$$

where  $\tau \approx 1/\Delta\omega \ll \mathcal{T}$  is the width of the  $I_b$  (*i.e.* background intensity) two-point function under the single filter scenario<sup>2</sup>. In arriving at ((53)) the form of  $\xi(t)$ , for the various orthonormal filter combinations depicted in Figure (1), are approximated as Gaussians of width  $n\tau$ , *viz.*

$$\xi(t) \approx \frac{\langle \mathcal{I}_b \rangle^2}{n} e^{-t^2 / (n^2 \tau^2)} \quad (54)$$

to enable a relatively simple analytic expression for ((53)).

To interpret the three terms on the right side of ((53)), the Dirac delta function in the first term is the abstract representation of a single channel spike of width  $2\pi/\mathcal{T}$  and height  $\mathcal{T}/(2\pi)$ ; thus the spectral amplitude of this term is

<sup>2</sup> The inequality is there to ensure that the limits of integration in ((50)) are effectively  $-\infty$  and  $\infty$  for the  $t$  integration of  $\xi(t)$  and  $\xi(t) \cos 2\Omega t$ , where  $t = t_2 - t_1$

$\epsilon_0^4 \langle I_b \rangle^2 \mathcal{T}^2 / 64$  which spans the single spectral channel of width  $\delta\omega = 2\pi/\mathcal{T}$  and centered at  $\omega = 2\Omega$ . The second term is also due to the presence of periodic signal, it has an amplitude  $\sqrt{\pi}\epsilon_0^4 \langle I_b \rangle^2 \mathcal{T}\tau/16$  which is smaller than the first term by the factor  $\approx \mathcal{T}/\tau \gg 1$ , and width  $\approx 1/(n\tau)$  which includes many channels because  $\mathcal{T} \gg n\tau$ . Evidently the first term is the tall and narrow ‘resonance line’ at frequency  $2\Omega$  that one can most readily detect as symptomatic (proof) of the periodic signal. Lastly the third term, a line centered at  $\omega = 0$  and also of width  $\approx 1/(n\tau)$ , is the background term, because being independent of  $\epsilon_0$  the line is there even in the absence of the periodic signal. However, when  $\Omega > 1/(n\tau)$  the signal line is located outside the Gaussian cutoff of this background line, and so the signal can still dominate the background even though the ratio of the former amplitude to the latter is  $\approx \epsilon_0^4 \mathcal{T}/\tau$  which might not be  $\gg 1$ . This is consistent with our earlier claim that the second criterion of ((49)) is also necessary for optimal signal detection. Since the proposed algorithm of using  $n \gg 1$  orthonormal filters enables the criterion to be satisfied more easily than the conventional single filter approach, it facilitates the recognition of embedded periodic or quasi-periodic transients.

#### 4.4. Noise in the power spectrum

It remains to compare the fluctuation amplitude of the power spectrum to the strength of the resonance line. As derived in Appendix B, the variance of the power spectrum emerges as

$$\begin{aligned} \text{var}(|\tilde{\mathcal{I}}(\omega)|^2) = & \langle \mathcal{I}_b \rangle^4 \frac{\pi^2 \epsilon_0^4}{4} \delta^2(\omega - 2\Omega) \left[ \frac{\sqrt{\pi} \epsilon_0^4 \mathcal{T} \tau}{16} e^{-n^2 \tau^2 (\omega - 2\Omega)^2 / 4} + \sqrt{\pi} \mathcal{T} \tau e^{-n^2 \tau^2 \omega^2 / 4} \right] \\ & + 2 \langle \mathcal{I}_b \rangle^4 \left[ \frac{\sqrt{\pi} \epsilon_0^4 \mathcal{T} \tau}{16} e^{-n^2 \tau^2 (\omega - 2\Omega)^2 / 4} + \sqrt{\pi} \mathcal{T} \tau e^{-n^2 \tau^2 \omega^2 / 4} \right]^2. \end{aligned} \quad (55)$$

In the absence of the periodic signal, *i.e.* when  $\epsilon_0 = 0$ , the variance reduces to

$$\text{var}(|\tilde{\mathcal{I}}(\omega)|^2) = 2\pi \langle \mathcal{I}_b \rangle^4 \mathcal{T}^2 \tau^2 e^{-n^2 \tau^2 \omega^2 / 2}, \quad (56)$$

which is exponentially small at the frequency of the signal  $\omega = 2\Omega$  if  $\Omega > 1/(n\tau)$ .

The ratio of the signal power to the standard deviation (standard error) in the power, or the first term of ((53)) divided by the square root of the first term of ((55)), is of order  $\mathcal{T}/\tau \gg 1$ , and is independent of  $n$ .

#### 4.5. Simulation of the sensitivity enhancement

A simulation is performed to test the performance of the orthonormal filters combination in detecting the embedded periodic signal of section 4.2. The parameters are  $\Omega = 33.3$  kHz and  $\epsilon_0^2 = 0.03$  for the signal,  $\sigma_\omega = 0.2$  MHz for the Gaussian spanned by the filter coefficients  $\mathbf{a}$ , and a carrier wave frequency (central frequency of the Gaussian filter, or equivalently  $\omega_0$ ) of 10 GHz. The value of  $\epsilon_0$  was chosen such that the signal is insignificant in the lower  $n$ -part series. For even smaller values of  $\epsilon_0$  the overall result of the simulation does not change. Except that for successively smaller values of  $\epsilon_0$  one would need to co-add more intensity series to find even weaker signals.

Results of the simulation are summarized in Table 2 and Figure 4, where it can be seen in the former that the signal-to-noise of the (intensity) power spectral density excess at the frequency  $2\Omega$  (the finite frequency mode of  $\sin^2 \Omega t$ ) increases monotonically with the number of filters combined. The latter power spectrum shows the line is clearly identifiable within the noise after successive filtering. Thus it can be seen that the simulation agrees well with the theory.

The results of section 4.2 apply to other time variable signals, for example a transient Gaussian pulse. The signal-to-noise ratio increases with the addition of  $n$  orthogonally filtered beams as  $\sqrt{n}$ . A Gaussian pulse of duration  $\sim 5\tau$  embedded in Gaussian noise was simulated and results are shown in Figure 5 and Table 3.

### 5. APPLICATION TO A VLA OBSERVATION OF PSR 1937+21

We now apply the noise reduction algorithm to a 10 minute observation of the millisecond pulsar PSR 1937+21 by the VLA on 21:36 UTC October 29, 2015. The voltage time series before processing comprise measurements at  $T = 15.625$  ns timing resolution. In the Fourier domain, the modes cover a frequency range of 32 MHz with equal weights, centered at 1.4 GHz. Owing to the wide frequency range, dispersion by the interstellar plasma is significant. Yet, following the recipe of the previous section, we minimized dispersion effects by filtering the voltage modes digitally with a narrow Gaussian of 0.663 MHz FWHM, corresponding by ((9)) to a Gaussian intensity autocorrelation function of 400 ns or 26 sampling intervals FWHM, to produce the intensity time series  $I_r$ . Specifically, from the published dispersion measure (DM) of 71 pc cm<sup>-3</sup> (Kaspi et al (1994)), the dispersive broadening during propagation through

Order of processing	Simulated line significance at $\omega=66.6$ kHz = $2\Omega$	Correlation length ( $\mu s$ )
1-part	2.8	12.0
2-part	1.8	24.0
3-part	1.7	36.0
4-part	2.9	48.0
5-part	7.4	60.0
6-part	8.1	72.0

**Table 2.** Simulation results for a 33.3 kHz period signal embedded in Gaussian background noise. Intensity series for 1-part to 6-part were simulated. The correlation length of the intensity data, shown in last column, increases with filter order  $n$  as  $n\tau$ , where  $\tau$  is the coherence time of the 1-part series.

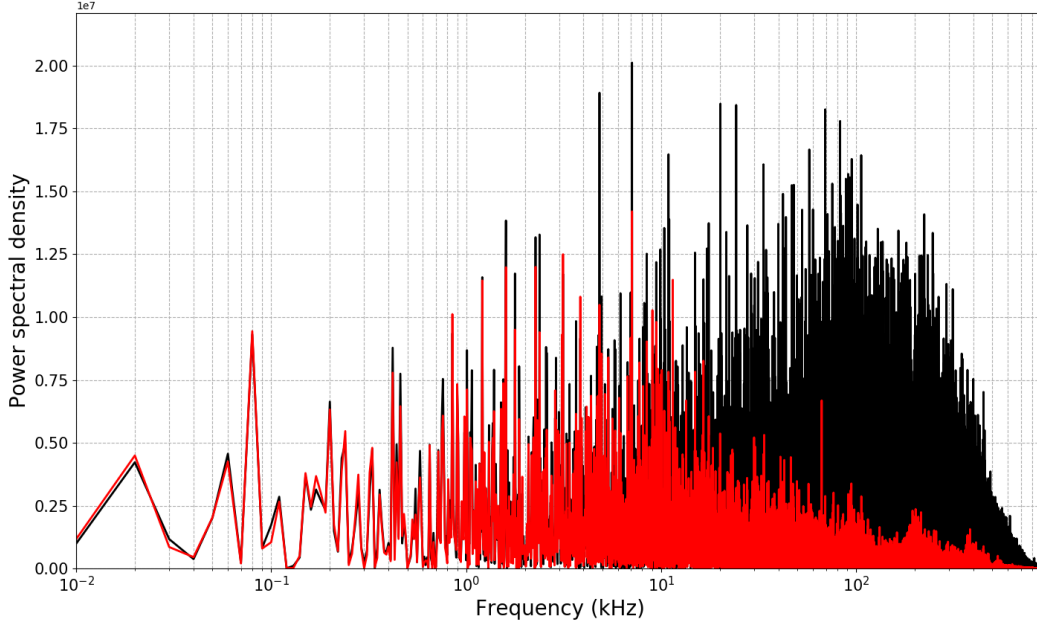


**Figure 4.** The simulated power spectral density of 1-part (black) and overlapping 6-part (red). The signal power is prominent in 6-part at frequency  $\omega = 66.6$  kHz, *i.e.* at twice the frequency  $\Omega = 33.3$  kHz of the embedded sine wave. Table 2 contains 1-part to 6-part line significances measured from the power spectral density data and correlation lengths of the intensities.

Order of processing	Simulated pulse significance	Signal-to-noise ratio
1-part	1.2	2.2
2-part	1.7	3.1
3-part	1.6	3.3
4-part	2.1	4.1
5-part	3.2	5.4
6-part	3.8	6.3

**Table 3.** Simulation results for a Gaussian pulse embedded in Gaussian background noise. Intensity series for 1-part to 6-part were simulated. Following the prediction of section 4.2, the signal-to-noise ratio increases with filter order  $n$  approximately as  $\sqrt{n}$ . The correlation lengths for 1-part to 6-part are the same as those found in Table 2.

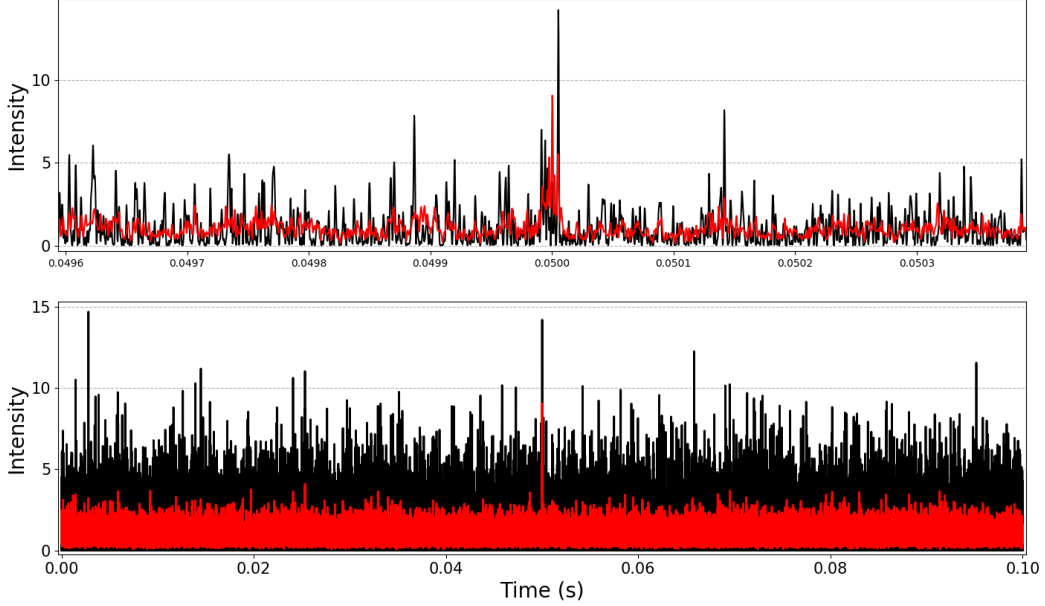


**Figure 5.** The simulated intensity time series of 1-part (black) and overlapping 6-part (red). The transient Gaussian pulse is visible and significant only in 6-part, as shown in the top figure and Table 3, respectively. The bottom figure shows the entire simulated time series, with Gaussian pulse embedded in the center. The signal-to-noise ratio of the Gaussian pulse increases roughly as  $\sqrt{n}$ . However, for even larger  $n$  we find  $\sqrt{n}$  sets a lower limit. For example, continuing to  $n = 21$ , the SNR is measured to be  $\sim 16$  which is greater than the predicted signal-to-noise increase of  $\sqrt{21} \times (\text{conventional } n = 1 \text{ SNR}) \sim 10$ . Significances and SNRs for  $n = 1$  through  $n = 6$  are shown in Table 3.

the interstellar medium is of order

$$\delta t = 142 \left( \frac{\text{DM}}{71 \text{ pc cm}^{-3}} \right) \left( \frac{\Delta \nu}{0.663 \text{ MHz}} \right) \left( \frac{1.4 \text{ GHz}}{\nu} \right)^3 \mu\text{s} \quad (57)$$

for the relevant bandwidth, 0.663 MHz, and is much smaller than the period of 1.56 ms (Kaspi et al (1994)). Thus the pulsar light curve is unaffected within such a small  $\Delta \nu$ .

### 5.1. Pulse profile

When the voltage data were digitally processed by the  $n$ -part filtering algorithm outlined in section 3 (with each part having the same Gaussian intensity bandwidth (see Figure (1)) of 0.663 MHz), the resulting intensity time series are shown in Figure refintensity for  $n = 1, 2, \dots, 5$ , where it can be seen that the relative noise variance at the resolution  $T$  comes down with increasing  $n$ . Even more precisely, Table 1 shows that the relative variance is  $1/n$ , consistent with the theoretical prediction of section 3, and the advantage of using an arbitrarily large  $n$  goes away when the time series is averaged over indefinitely large time intervals  $\mathcal{T} = NT$  with  $N \gg n$ . This too is consistent with theory, as is the broadening of the intensity autocorrelation function with  $n$  which provides the explanation of why the relative variance for  $n > 1$  goes down with increasing  $\mathcal{T}$ , Figure 3.

To assess the performance in pulsar detection, the resulting  $n$ -part intensity time series were folded a modulo the 1.56 ms period of PSR 1937+21. In Figure 2 is shown a comparison of the pulse profiles of  $n = 1$  against  $n = 6$  at various timing resolution. In accordance with expectation, it can be seen that the original (and highest) resolution data has the best signal-to-noise advantage in revealing the presence of pulsations when  $n = 6$ . The shape of the pulse profile is consistent with the primary and inter-pulse configuration reported in the literature (e.g. Kaspi et al (1994)). To quantitatively test whether the signal-to-noise enhancement of the pulse profile is real, we computed the ACF of the pulse profile for various  $n$  ranging from  $n = 1$  to  $n = 5$ , with ACFs for  $n = 1$  to  $n = 3$  shown in Figure 3, and evaluated the statistical significance of the correlation using the Pearson  $p$ -statistic. The results are presented in

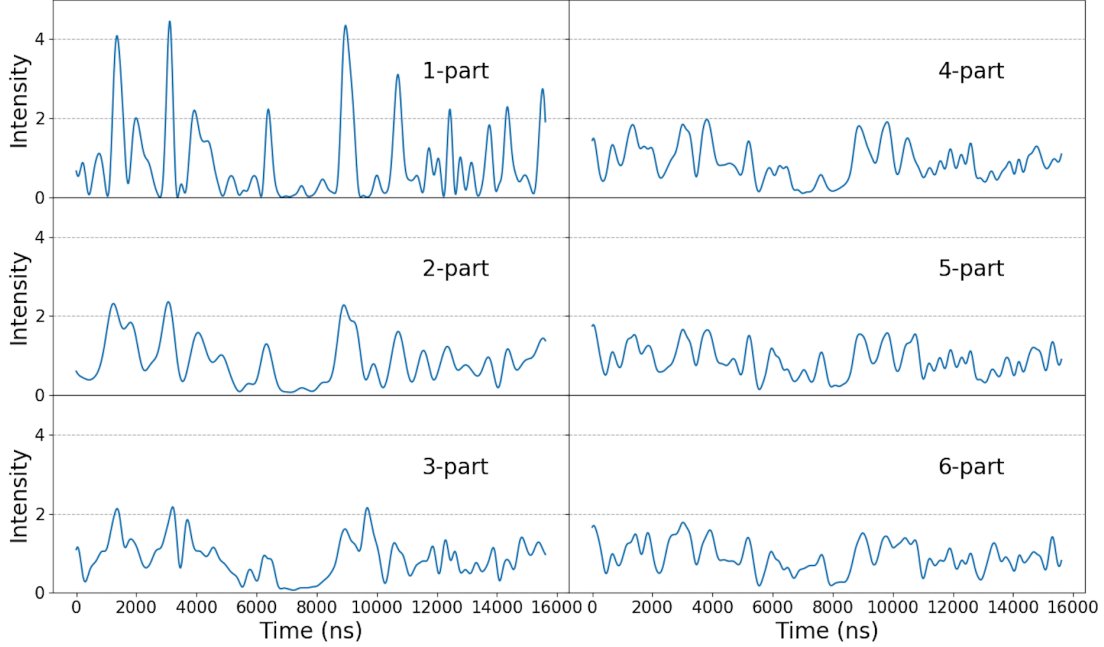


**Figure 6.** A small segment of the pulsar light curve, with amplitude filtered digitally in the conventional way by a narrow Gaussian bandpass (1-part), and by  $n$  multiple filters with  $n \leq 6$ . The filters' designs were explained in section 3 and illustrated in Figure (1). The intensity of each series was normalized to a mean of unity, and the sampling time is  $T = 15.625$  ns. Note the progressive decrease in the noise variance, accompanied by an increase in the noise coherence time, as  $n$  increases.

Tables 4 and 5 for raw (unbinned) data, as well as binned data to ensure all points are independent even for  $n = 5$ . It can be seen that for the unbinned data where the resolution is highest, the significance of the correlation is largest for  $n = 5$  and decreasing monotonically to  $n = 1$ . Same is true also for the binned data, although the improvement in the correlation coefficient is less because the noise reduction advantage of  $n > 1$  scenarios is meant to be absent (or substantially reduced) here.

Since our proposed methodology is best suited for detecting signals that vary on short timescales, but the pulsar modulation of the intensity occurs on timescales far larger than the ACF width of any of the  $n$  orthogonal filter combinations employed, the significance enhancement w.r.t.  $n$  is indicative of the presence of periodic or quasi-periodic modulations on small timescales.

### 5.2. Power spectrum of the pulse profile - microstructures

Thus the next question is whether the suppression of noise in high timing resolution as offered by the proposed analysis technique could result in the discovery of fast transient emissions in the pulse profile that become averaged away in low resolution data. To investigate, we computed the power spectral density (PSD) of the pulse profile, with ensuing frequencies necessarily quantized into multiples of the pulsar frequency.

In sections 4.1 – 4.4 and the simulation of section 4.5, we showed the variance of the noise spectral density decreases with filter order  $n$ . In Figure 7 we observe this behavior in the power spectra of the filtered and stacked intensity data. The spectrum frequency spacing is  $\omega_p$ , where  $\omega_p$  is the pulse frequency. Correspondingly, every peak in the spectrum is the location of a potential pulsar harmonic line.

We restrict our search to slow modulations that take place on timescales  $\gg 1/\Delta\nu$  where  $\Delta\nu \approx 0.7$  MHz, since

Order of processing	Autocorrelation coefficient	Degrees of freedom	Null hypothesis acceptance probability	Significance of correlation
1-part	0.135	2392	$1.69 \times 10^{-11}$	$6.83\sigma$
2-part	0.208	1196	$1.86 \times 10^{-13}$	$7.45\sigma$
3-part	0.256	797	$1.08 \times 10^{-13}$	$7.52\sigma$
4-part	0.310	598	$4.36 \times 10^{-15}$	$7.93\sigma$
5-part	0.349	478	$1.94 \times 10^{-15}$	$8.03\sigma$

**Table 4.** The autocorrelation coefficient and statistical significance of the pulsar intensity profile in the original resolution of 15.625 ns and at the time lag of 4,000 resolution elements, *viz.* 62.5  $\mu$ s. Conversion from coefficient to significance was performed using the Student  $t$ -distribution and the Pearson  $p$ -statistic, see *e.g.* Chapter 14 of [Press et al \(2007\)](#). The degrees of freedom were evaluated by taking account of the larger correlation lengths of the  $n$ -part intensity series (section 3 and Figure 3).

Order of processing	Autocorrelation coefficient	Null hypothesis acceptance probability	Significance of correlation
1-part	0.497	$9.38 \times 10^{-33}$	$11.98\sigma$
2-part	0.512	$6.75 \times 10^{-35}$	$12.38\sigma$
3-part	0.521	$3.09 \times 10^{-36}$	$12.62\sigma$
4-part	0.539	$3.64 \times 10^{-39}$	$13.14\sigma$
5-part	0.579	$2.96 \times 10^{-46}$	$14.33\sigma$

**Table 5.** The autocorrelation coefficient and statistical significance of a binned pulsar intensity profile with the lower resolution of 3.125  $\mu$ s (or 200 original time bins) and at the time lag of 62.5  $\mu$ s. Conversion from coefficient to significance was performed using the Student  $t$ -distribution and the Pearson  $p$ -statistic, see the caption of the previous figure. The degrees of freedom equal the number of data points that participated in the computation of correlation coefficient because the points are all independent of each other after binning.

timescales nearing  $1/\Delta\nu$  are affected by dispersion of the interstellar medium. Specifically by ((57)) the time delay across the entire bandwidth  $\Delta\nu$  of 0.663 MHz is  $\approx 142 \mu$ s, but because the frequency spread of the sought modulations is a much smaller fraction of the observer’s  $\Delta\nu$ , such effects survive dispersive broadening. On the other hand, the lowest frequency region of the pulse profile PSD is dominated in power by the lower-order pulsar harmonic lines. There is not enough background data in this regions to properly test these lines against the theory. This prevents the search of low harmonic lines.

By visual inspection of the pulse profile PSD we identified the 83<sup>rd</sup> pulsar harmonic line and subsequently tested the line against the theory. Table 6 contains the line significance as a function of filter order, from the PSD of ten minutes of stacked profile data, up to 6<sup>th</sup> processing order. The line is insignificant in 1-part, but the noise is sufficiently reduced to reveal an  $\sim 8\sigma$  line in 6-part. Figure (8) shows that the harmonic line is buried in the noise in 1-part and becomes prominent as the noise is suppressed, in 6-part.

Order of processing	53.9 kHz line significance	Correlation length ( $\mu$ s)
1-part	0.55	0.6250
2-part	0.73	1.250
3-part	1.64	1.875
4-part	2.66	2.500
5-part	4.96	3.125
6-part	7.84	3.750

**Table 6.** Significance of the 83<sup>rd</sup> pulsar harmonic line, as a function of filter order, from the power spectral density of ten minutes of stacked intensity data. Spectra for 1-part and 6-part are compared for ten minutes of profile data in Figure (8).

## 6. APPLICATION TO LIGO BINARY BLACK HOLE MERGER EVENT GW150914

Another application of the ‘eigen-filter’ (orthogonal filtering) algorithm presented above attempts to increase the search sensitivity of transient gravitational-wave (GW) events. Short-lived bursts of GWs are the primary target application; in particular, bursts of GW radiation detectable over a few coherence times, which are unanticipated,



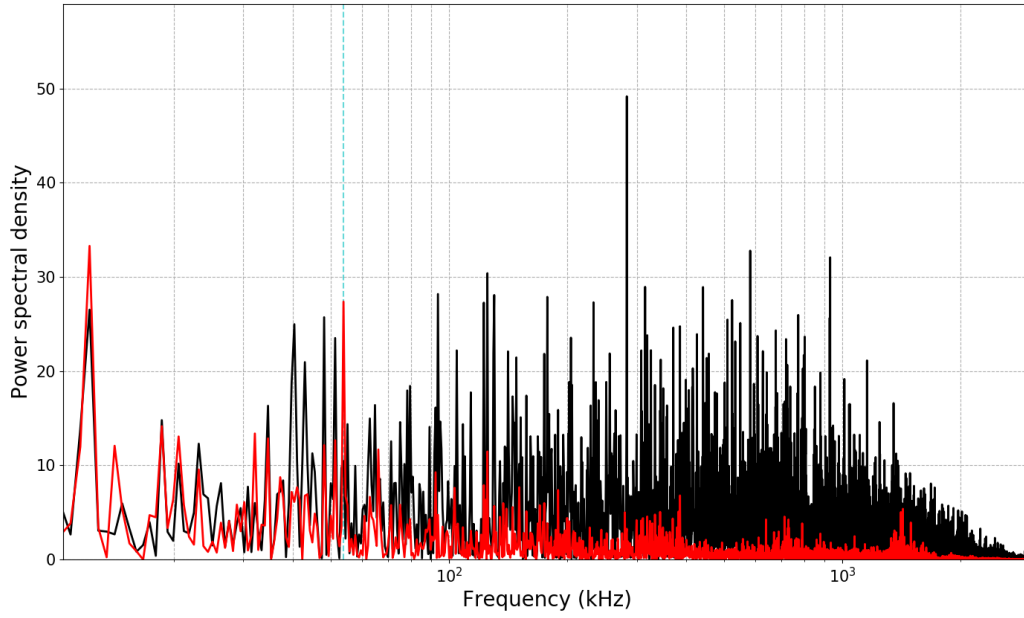


**Figure 7.** The power spectral density of ten minutes of stacked pulsar data, 1-part (black) and overlapping 6-part (red). The vertical dashed line shows the location of the 53.9 kHz pulsar harmonic.

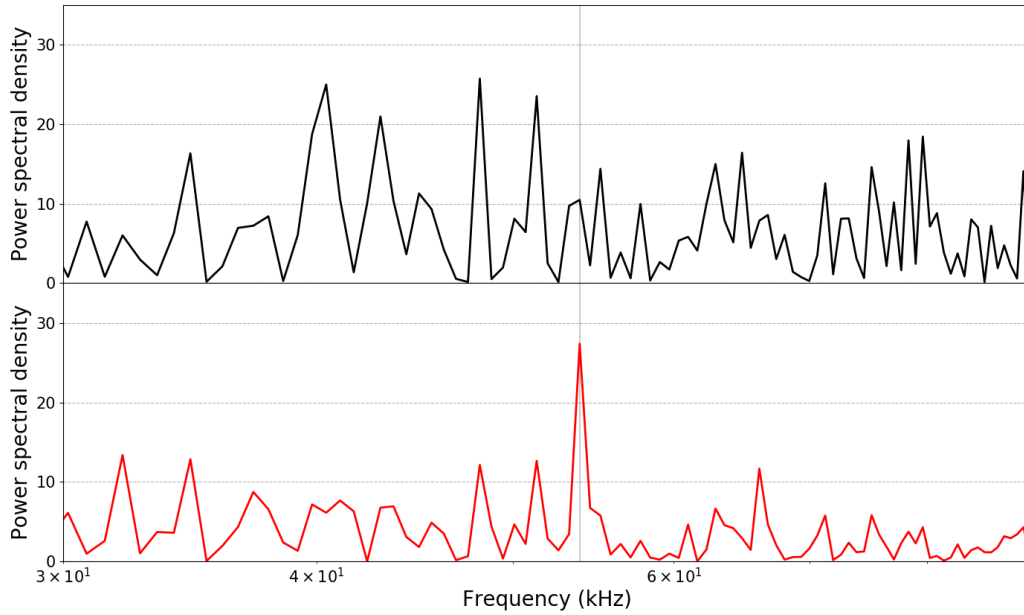


**Figure 8.** The top and bottom figures are, respectively, the 1-part and 6-part power spectral density of ten minutes of pulse profile data. The line is insignificant in 1-part and one must process the data with digital filters to ‘uncover’ it. Table 6 contains line significances for 1-part through 6-part. The 53.918 kHz harmonic line is highlighted with a vertical grey line.



*i.e.* where the theoretical waveform is unknown. In the first and second observing runs, the Laser Interferometer Gravitational-Wave Observatory (LIGO; [Abramovici et al \(1992\)](#)) in the US and Italy’s Virgo ([Accadia et al \(1992\)](#)) have confidently detected transient GWs from sources with known waveform models, namely merging black hole binaries (BBH) and merging neutron stars ([Abbott et al \(2019a\)](#)). Japan’s Kamioka Gravitational-Wave Detector (KAGRA; [Aso et al \(2013\)](#)) is scheduled to join in the latter part of the third observing run, O3, which concludes April 30, 2020. At times and frequencies where non-stationary, non-Gaussian noise sources are absent, for example glitches, the LIGO data streams are statistically locally stationary and Gaussian [Abbott et al \(2019b\)](#). Noise of this character masks weak embedded GW signals, of any form, at all times, but it is precisely this time-independence that permits its systematic reduction.

One method to find weakly modeled, or unmodeled candidate GW bursts, is with analysis algorithm Coherent WaveBurst (cWB) ([Klimenko et al \(2008\)](#) and [Klimenko et al \(2016\)](#)), currently in use by LIGO-Virgo collaboration. The cWB algorithm incorporates both excess power and cross correlation between detector pairs to identify triggers. Here we show excess power stands to gain a  $\sim \sqrt{n}$  increase over Gaussian noise power.

Low latency pipelines and multi-messenger astronomy also stand to benefit. The likelihood of a weak signal classifying as a trigger while the instruments are online could go up, if increased SNR in both detectors and increased correlation between detector pairs with filter order  $n$  are found. Then electromagnetic observing partners could be alerted to triggers that might otherwise only be found in offline mode. Of course, the technique presented here in no way renders any less critical the work performed to exclude as astrophysical non-stationary, non-Gaussian transient noise events. For ground-based detectors, these noise sources can be the cause of global-scale environmental influences and detector noise. For example, coincident noise triggers, which are not infrequent, may also correlate in time. ([Abbott et al \(2016a\)](#))

As proof-of-principle, we apply eigen-filtering to the first BBH merger event, GW150914, detected by LIGO ([Abbott et al \(2016b\)](#)). We use 32 seconds of publicly available LIGO strain data surrounding the event from Livingston and Hanford, obtained from the [LIGO Scientific Collaboration and Virgo Collaboration \(2017\)](#). The data have bandwidth 2048 Hz and are sampled at the Nyquist rate, 4096 Hz. GW150914 falls under the category of transients whose SNR is maximized by applying a matched filter, constructed from known waveform templates, to the data streams of each detector separately. For that reason, SNRs for GW150914 reported in the literature are larger than those computed from excess power alone.

First, we describe the data pre-conditioning and how the eigen-filters are constructed for specific application to LIGO data, the strain data are first whitened, so  $\sigma_I^2/\bar{I}^2$ , for the  $n^{\text{th}}$  intensity series, is  $\sim 2/n$ . Symmetry of the eigen-filters across the BW of interest is required to satisfy condition ((31)) as close to identically as possible. A ‘first order approach’ to enforcing symmetry, however, is to apply an eigen-filter with a boxcar profile to the original BW, *i.e.* we do not bandpass the data. For our demonstration, this is an acceptable starting point. One must also keep in mind, any applied filter BW must be  $\gg$  than the signal frequency for eigen-filtering to successfully corroborate theoretical prediction. For GW150914 the signal frequency spans approximately one decade, between 30 and 300 Hz. After these two operations, we measure a finite non-zero correlation length that increases with filter order  $n$  as  $n\tau$ , where  $\tau$  is the correlation length of the  $n=1$  intensity series. Results for the Hanford and Livingston event significance and SNR as a function of filter order are shown in Table (6).

We also cross correlate LIGO Hanford and Livingston eigen-filtered intensity data streams for a total of 0.1 seconds preceding the reported ‘merger end time’. The known delay time between Hanford and Livingston is recovered. The merger event in Hanford’s detector stream lags  $\sim 7$  ms behind that in Livingston’s. Increased correlation with filter order is shown in Figure (10). The same result holds when larger segments of data are cross correlated.

Additionally, there will be a significant source of Gaussian noise from astrophysical populations in future space based Laser Interferometer Space Antenna (LISA; [Amaro-Seoane et al \(2017\)](#))<sup>3</sup>. At mHz frequencies a confusion noise from tens of millions of unresolved ultra-compact Galactic binaries (UCBs) ([Littenberg et al \(2019\)](#)) is expected. The superposition of many UCBs, each emitting primarily monochromatic GWs at a particular frequency and random phase, constitute an effective stochastic foreground noise. The superposed UCB signals constitute a Gaussian noise time series with faint, resolvable GW signals embedded. Reducing this noise will allow one to more easily sift transient, extragalactic signals occupying the same frequency band.

Moreover, [Abbott et al \(2016c\)](#) show in Figure 1a the estimated stochastic GW background from the extragalactic population of binary black holes is present in the ground-based data streams. Though interesting in its own right, this background will be a significant noise source in the LISA data stream *i.e.* if one extends the spectrum into the LISA

<sup>3</sup> LISA is currently under active development, <https://www.elisascience.org/>.

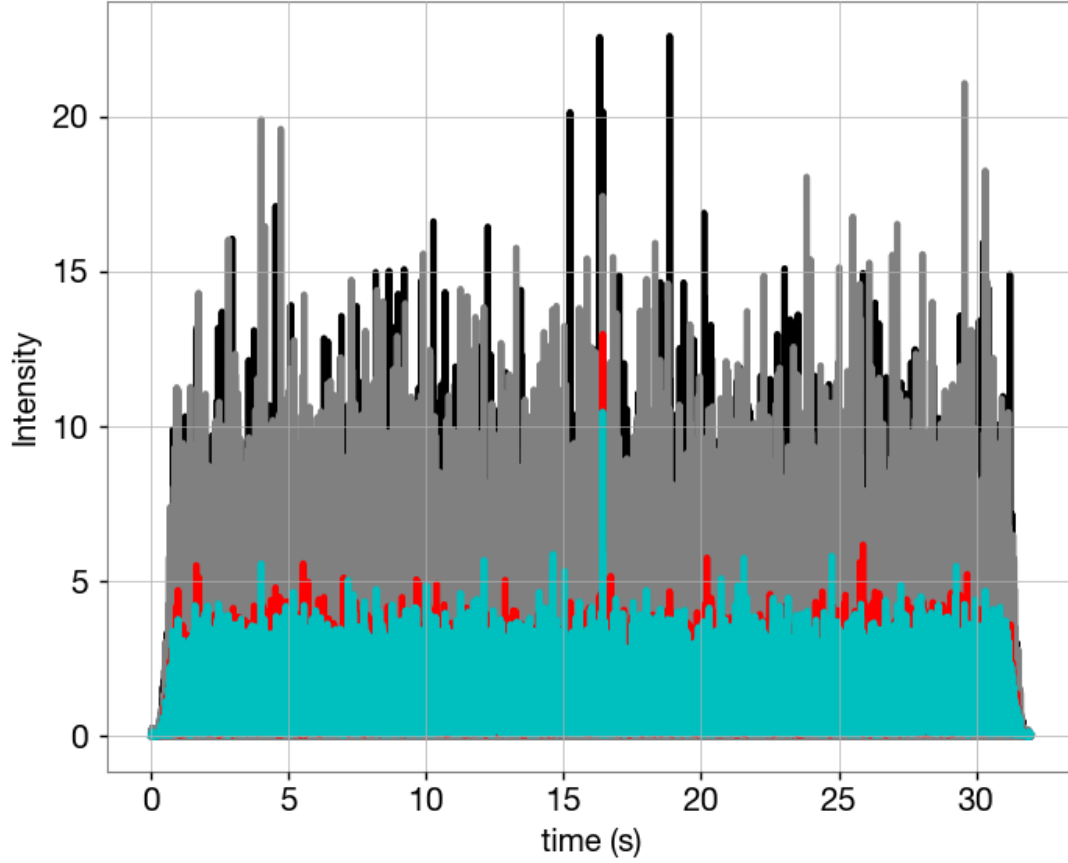


**Figure 9.** Intensity time series of 1-part (Hanford, black; Livingston, grey) and overlapping 6-part (Hanford, red; Livingston, cyan). The transient GW event clearly rises above the noise in 6-part. The signal-to-noise ratio of the event increases roughly as  $\sqrt{n}$

Order of processing	Significance Hanford	Signal-to-noise ratio Hanford	Significance Livingston	Signal-to-noise ratio Livingston	Correlation length (ms)
1-part	1.4	2.1	0.9	1.6	0.2
2-part	1.9	2.9	1.3	2.3	0.4
3-part	2.3	3.6	1.6	2.8	0.6
4-part	2.7	4.1	1.8	3.2	0.8
5-part	2.9	4.5	2.0	3.5	1.0
6-part	3.1	4.9	2.1	3.9	1.2

**Table 7.** GW150914 excess power signal-to-noise ratios and significances, for co-added intensity series processed by  $n = 1$  to  $n = 6$  eigen-filters. SNR increases approximately as  $\sqrt{n}$ . Correlation length increases as  $n\tau$ , where  $\tau$  is the correlation length of the  $n=1$  intensity series. The SNR is computed as the mean intensity over noise for 30 ms surrounding the peak intensity, specifically between UTC 1126259462.41 and 1126259462.44 for Hanford. The same length interval is used for Livingston, but with averaging window shifted 7 ms to earlier times, corresponding to the GW's earlier arrival time at the Livingston detector.

band as  $f^{2/3}$ . In principle, these foreground and background Gaussian noise sources are reducible in GW intensity time series with the algorithm presented above, allowing one greater search sensitivity for unexpected, short-duration GW bursts.

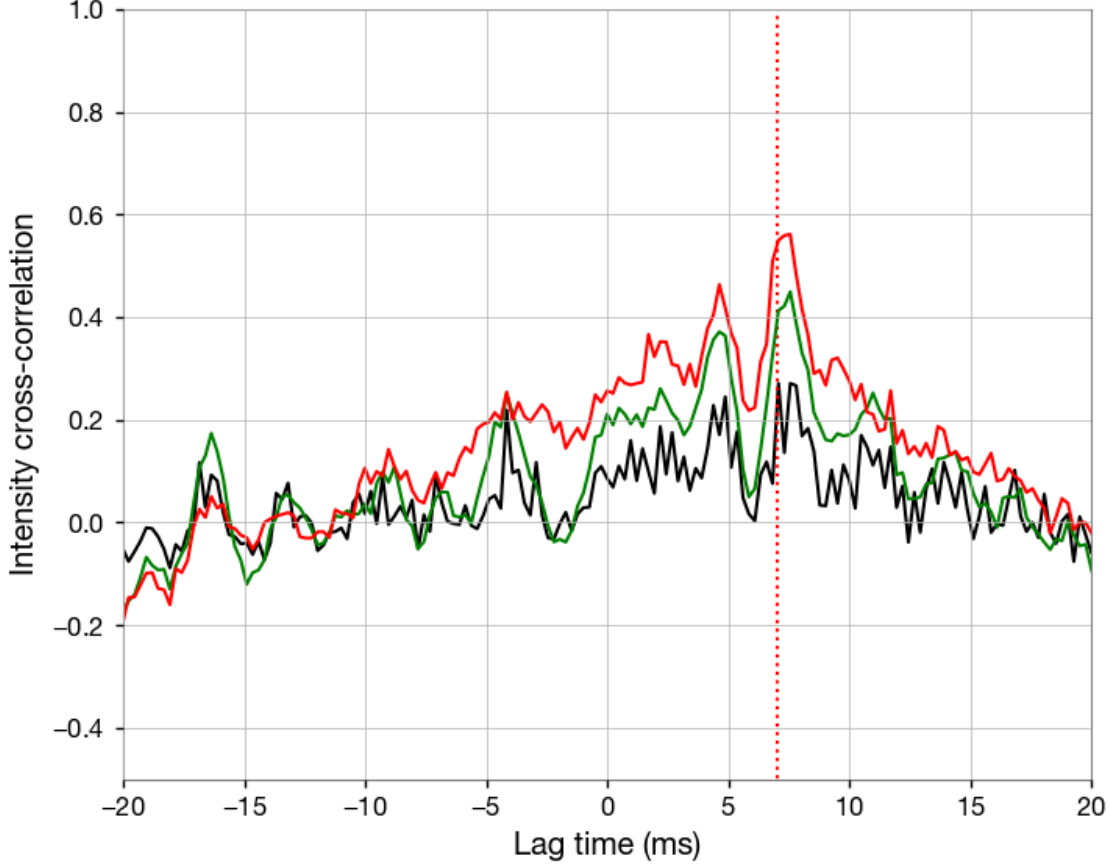


**Figure 10.** The 0.1 seconds leading up to the end of merger were cross correlated between Hanford and Livingston eigen-filtered intensity time series. Correlation increases with filter order  $n$ . Respectively, black, green and red curves correspond to co-added intensity series  $n=1,3$  and 6. The vertical dashed red line marks the 7 ms lag time, which is within the peak cross correlation for each intensity series.

## 7. CONCLUSION

An algorithm is proposed to significantly reduce the Gaussian noise of radio intensity time series by digitally designing  $n$  amplitude filters, where  $n \geq 1$  is arbitrarily large, having identical intensity bandwidths such that the resulting co-added intensity time series has relative variance  $\approx 1/n$  on timescales  $\lesssim$  the coherence time of the noise, but recovers to the limit set by the radiometer equation ((21)) in the opposite limit of long timescales as required by the Cramers-Rao bound (Nair & Tsang (2015)).

The method is applied to a 10 minute VLA observation of the millisecond pulsar PSR 1937+21 at the resolution of  $T = 15.625$  ns and FWHM intensity bandwidth  $\Delta\nu = 0.663$  MHz. It is found that even when  $n$  is as low as  $n \approx 5$  the pulsar intensity profile has much lower noise than the conventional single filter scenario (for equal  $\Delta\nu$  in both cases) unless the time series are bin averaged to a resolution much poorer than  $n/\Delta\nu \approx n\tau$ . In this way, faint transient signals that occur on timescales between  $\tau$  and  $n\tau$  are enhanced with respect to noise. The existence of a 53.9 kHz periodic modulation (corresponding to the 83<sup>rd</sup> pulsar harmonic) in the intensity pulse profile is revealed only by applying  $n > 3$  filter combinations.

Since the advantage exists only at high resolution, the algorithm is best suited to the search of faint and fast transients that would otherwise be smeared out by any noise suppression scheme involving time averaging.

Lastly we applied the algorithm to the first gravitational wave event detected by LIGO. We found the intensity signal-to-noise ratio of the event increases roughly as  $\sqrt{n}$ . We demonstrate the cross correlation between the Hanford

and Livingston intensity series for 0.1 s preceding the merger's end time increases with filter order  $n$ .

The authors are grateful to Paul Demorest, Barry Clark, and Jean Eilek at NRAO Socorro for helpful discussions, and to Paul Demorest for providing the VLA data of PSR 1937+21. KL is also grateful to Peter Bender for bringing attention to a population of unresolved extragalactic binary black holes as a potential source of noise for LISA. KL's research was supported by an appointment to the NASA Postdoctoral Program at the NASA Marshall Space Flight Center, administered by Universities Space Research Association under contract with NASA.

## REFERENCES

- LIGO, Virgo Scientific collaboration, B. P. Abbott et al., PRL, 116, 061102  
 LIGO, Virgo Scientific collaboration, B. P. Abbott et al., CQG 33, 13  
 LIGO, Virgo Scientific collaboration, B. P. Abbott et al., PRL 116, 131102  
 LIGO, Virgo Scientific collaboration, B. P. Abbott et al., PRLX 9, 031040  
 LIGO, Virgo Scientific collaboration, B. P. Abbott et al., ArXiv e-prints, 1908.11170  
 Abramovici, A. et al., 1992, Science 256, 5055  
 Accadia, T. et al., 2012, JINST, 7, 3  
 Amaro-Seoane, P. et al., ArXiv e-prints, arXiv:1702.00786  
 Aso, Y. et al., 2013, PRD, 88, 4  
 Burke, B.F., & Graham-Smith, F., 2010, An Introduction to Radio Astronomy, 3rd edition, Cambridge University Press.  
 Christiansen, W.N., & Högbom, J.A., 1985, Radio Telescopes, 2nd edition, Cambridge University Press.  
 LIGO Scientific Collaboration and Virgo Collaboration 2017 Gravitational Wave Open Science Center: Available catalogs URL <https://doi.org/10.7935/82H3-HH23>  
 Klimenko, S, 2008 CQG, 25, 11  
 Klimenko, S, 2016 PRD, 93, 042004  
 Kaspi, V. M., Taylor, J. H., & Ryba, M. F. 1994, ApJ, 428, 713  
 Lieu, R., 2017, ApJ, 844, 50  
 Littenberg, T., et al., 2019, ArXiv e-prints, arXiv:1903.05583  
 Loudon, R., 2000, The quantum theory of light, 3rd edition, Oxford  
 Nair, R., and Tsang, M., 2015, ApJ, 808, 125  
 Press, W.H., Teukolsky, S.A., Vetterling, W.T., & Flannery, B.P., 2007, Numerical Recipes, 3rd ed., C.U.P.  
 Wang, L.J., Magill, B.E., & Mandel, L., 1989, JOSA B, 6, 964

## APPENDIX

### A. VALIDITY OF THE RADIOMETER EQUATION AS APPLIED TO LONG TERM INTENSITY AVERAGING

When the narrow band filter coefficients  $\{a_j\}$  digitally multiply the voltages of an incident radiation beam with a flat intensity spectrum, and the exercise is repeated using another set of narrow band coefficients  $\{b_j\}$ , the two ensuing intensity series were denoted by  $I_r$  and  $I'_r$  in section 3, while the summed intensity  $\mathcal{I}_r = I_r + I'_r$  was shown to possess 50 % less relative variance than  $I_r$  or  $I'_r$  individually. Despite this apparent advantage the radiometer equation governing the relative variance of the sample mean intensity taken over many contiguous coherence times was shown to remain valid under the scenario of two specific Gaussian-type filters  $\{a_j\}$  and  $\{b_j\}$ . In this Appendix we demonstrate the validity of the radiometer equation for *any* filters  $\{a_j\}$  and  $\{b_j\}$ .

We begin with by substituting ((34)) into ((19)) and evaluating one of the double summations as an integral (the other summation then assumes the value  $N$ ), *viz.*

$$\begin{aligned}
 \text{var}(\mathcal{I}_T) &= \frac{1}{N^2} \sum_{r,s=1}^N \text{cov}(\mathcal{I}_r, \mathcal{I}_s) \\
 &= \frac{\mathcal{T}^2}{NT} \int \{[a(\omega)a^*(\omega')]^2 + [b(\omega)b^*(\omega')]^2 + 2a(\omega)a^*(\omega')b(\omega)b^*(\omega')\} e^{-i(\omega-\omega')t} d\omega d\omega' dt \\
 &= \frac{2\pi\mathcal{T}^2}{NT} \int \{[a(\omega)a^*(\omega')]^2 + [b(\omega)b^*(\omega')]^2 + 2a(\omega)a^*(\omega')b(\omega)b^*(\omega')\} \delta(\omega - \omega') d\omega d\omega' \\
 &= \frac{2\pi\mathcal{T}^2}{NT} \int [|a(\omega)|^2 + |b(\omega)|^2]^2 d\omega \\
 &\approx \frac{\tau}{NT} (\langle I_r \rangle + \langle I'_r \rangle)^2,
 \end{aligned} \tag{A1}$$

In arriving at the last step use was made of ((13)) and the approximation

$$\mathcal{T}^2 \int |a(\omega)|^4 d\omega \approx \frac{\langle I_r \rangle^2}{\Delta\omega} \approx \langle I_r \rangle^2 \tau. \tag{A2}$$

Thus  $\text{var}(\mathcal{I}_T)/\langle \mathcal{I} \rangle^2 \approx \tau/(NT)$ , consistent with the radiometer equation ((21)).

## B. POWER SPECTRUM OF THE INTENSITY AND ITS NOISE

The power spectral amplitude  $\tilde{\mathcal{I}}(\omega)$  of intensity fluctuation is the Fourier transform of the (stochastic) intensity time series  $\mathcal{I}(t)$ . The modulus square of  $\tilde{\mathcal{I}}(\omega)$  is the power spectrum

$$|\tilde{\mathcal{I}}(\omega)|^2 = \int dt_2 \int dt_1 e^{i\omega(t_2-t_1)} \mathcal{I}(t_1) \mathcal{I}(t_2). \quad (\text{B1})$$

Changing the variable  $t_2$  to  $t$  where  $t = t_2 - t_1$ , and taking the expectation (ensemble average) value, we have

$$\begin{aligned} \langle |\tilde{\mathcal{I}}(\omega)|^2 \rangle &= \int dt_1 e^{-i\omega t_1} \int dt_2 e^{i\omega t_2} [\langle \mathcal{I}(t_1) \mathcal{I}(t_2) \rangle - \langle \mathcal{I}(t_1) \rangle \langle \mathcal{I}(t_2) \rangle] \\ &\quad + \int dt_1 e^{-i\omega t_1} \int dt_2 e^{i\omega t_2} \langle \mathcal{I}(t_1) \rangle \langle \mathcal{I}(t_2) \rangle \end{aligned} \quad (\text{B2})$$

where, by ((45)) and such equations as ((46)) and ((47)),

$$\langle \mathcal{I}(t_1) \mathcal{I}(t_2) \rangle - \langle \mathcal{I}(t_1) \rangle \langle \mathcal{I}(t_2) \rangle = \xi(t_2 - t_1) (1 + \epsilon_0^4 \sin^2 \Omega t_1 \sin^2 \Omega t_2), \quad (\text{B3})$$

and

$$\langle \mathcal{I}(t_1) \rangle \langle \mathcal{I}(t_2) \rangle = \langle \mathcal{I}_b \rangle^2 (1 + \epsilon_0^2 \sin^2 \Omega t_1 + \epsilon_0^2 \sin^2 \Omega t_2 + \epsilon_0^4 \sin^2 \Omega t_1 \sin^2 \Omega t_2), \quad (\text{B4})$$

with  $\xi(t)$  as defined in ((52)).

The subsequent evaluation of the integrals was already performed in that portion of the main text around ((52)), resulting in ((53)) as the expression for  $|\tilde{\mathcal{I}}(\omega)|^2$  in the vicinity of  $\omega = 2\Omega$ . Specifically at and around  $\omega = 2\Omega$ ,

$$\begin{aligned} \int dt_1 e^{-i\omega t_1} \int dt_2 e^{i\omega t_2} \text{cov} [\mathcal{I}(t_1), \mathcal{I}(t_2)] &= \langle \mathcal{I}_b \rangle^2 \left[ \frac{\sqrt{\pi} \epsilon_0^4 \mathcal{T} \tau}{16} e^{-n^2 \tau^2 (\omega - 2\Omega)^2 / 4} + \sqrt{\pi} \mathcal{T} \tau e^{-n^2 \tau^2 \omega^2 / 4} \right] \\ &\quad + \dots, \end{aligned} \quad (\text{B5})$$

and

$$\int dt_1 e^{-i\omega t_1} \int dt_2 e^{i\omega t_2} \langle \mathcal{I}(t_1) \rangle \langle \mathcal{I}(t_2) \rangle = \langle \mathcal{I}_b \rangle^2 \frac{\pi^2 \epsilon_0^4}{16} \delta^2(\omega - 2\Omega) + \dots, \quad (\text{B6})$$

where  $\text{cov} [\mathcal{I}(t_1), \mathcal{I}(t_2)] = \langle \mathcal{I}(t_1) \mathcal{I}(t_2) \rangle - \langle \mathcal{I}(t_1) \rangle \langle \mathcal{I}(t_2) \rangle$  the missing terms represented by ‘ $\dots$ ’ apply only to the scenario of  $\omega = 0$ , a frequency far away from  $2\Omega$ , via at least one factor of  $\delta(\omega)$  in these terms.

To calculate the expectation value of the variance of  $|\tilde{\mathcal{I}}(\omega)|^2$ , *viz.*

$$\begin{aligned} \text{var}(|\tilde{\mathcal{I}}(\omega)|^2) &= \langle \tilde{\mathcal{I}}(\omega) \tilde{\mathcal{I}}^*(\omega) \tilde{\mathcal{I}}(\omega) \tilde{\mathcal{I}}^*(\omega) \rangle - \langle \tilde{\mathcal{I}}(\omega) \tilde{\mathcal{I}}^*(\omega) \rangle^2, \\ &= \int dt_1 e^{-i\omega t_1} \int dt_2 e^{i\omega t_2} \int dt_3 e^{-i\omega t_3} \int dt_4 e^{-i\omega t_4} \langle \mathcal{I}(t_1) \mathcal{I}(t_2) \mathcal{I}(t_3) \mathcal{I}(t_4) \rangle \\ &\quad - \langle \tilde{\mathcal{I}}(\omega) \tilde{\mathcal{I}}^*(\omega) \rangle^2, \end{aligned} \quad (\text{B7})$$

where  $\langle \mathcal{I}(t_1) \mathcal{I}(t_2) \mathcal{I}(t_3) \mathcal{I}(t_4) \rangle$  is a voltage 8-point function of the form  $\langle V_1 V_2 V_3 V_4 V_5 V_6 V_7 V_8 \rangle$  with  $V_1 = V(t_1)$ ,  $V_2 = V^*(t_1)$ ,  $V_3 = V(t_2)$ ,  $V_4 = V^*(t_2)$  etc. In this notation only 10 of the 24 different contraction patterns contribute significantly to the integral of ((B7)) at frequencies in the vicinity of  $\omega = 2\Omega$  with  $\Omega$  satisfying ((49)). They are as follows.

Firstly, one single contraction (1, 2)(3, 4)(5, 6)(7, 8) that yields  $\langle \mathcal{I}(t_1) \rangle \langle \mathcal{I}(t_2) \rangle \langle \mathcal{I}(t_3) \rangle \langle \mathcal{I}(t_4) \rangle$ , contributing the quantity

$$\alpha = \langle \mathcal{I}_b \rangle^4 \left[ \frac{\pi^2 \epsilon_0^4}{16} \delta^2(\omega - 2\Omega) \right]^2 \quad (\text{B8})$$

to the integral of ((B7)).

Secondly, six contractions (1, 2)(3, 4)(5, 8)(6, 7), (1, 4)(2, 3)(5, 6)(7, 8), (1, 2)(3, 6)(4, 5)(7, 8), (1, 6)(2, 5)(3, 4)(7, 8), (1, 8)(2, 7)(3, 4)(5, 6), and (1, 2)(3, 8)(4, 7)(5, 6), each yielding a term of the form  $\langle \mathcal{I}(t_1) \rangle \langle \mathcal{I}(t_2) \rangle \text{cov} [\mathcal{I}(t_3), \mathcal{I}(t_4)]$  or  $\langle \mathcal{I}(t_3) \rangle \langle \mathcal{I}(t_4) \rangle \text{cov} [\mathcal{I}(t_1), \mathcal{I}(t_2)]$  or other arrangements, and anyone of such terms contribute the quantity

$$\beta = \langle \mathcal{I}_b \rangle^4 \frac{\pi^2 \epsilon_0^4}{16} \delta^2(\omega - 2\Omega) \left[ \frac{\sqrt{\pi} \epsilon_0^4 \mathcal{T} \tau}{16} e^{-n^2 \tau^2 (\omega - 2\Omega)^2 / 4} + \sqrt{\pi} \mathcal{T} \tau e^{-n^2 \tau^2 \omega^2 / 4} \right] \quad (\text{B9})$$

to the integral of ((B7)).

Thirdly, three contractions  $(1, 4)(2, 3)(5, 8)(6, 7)$ ,  $(1, 8)(2, 7)(3, 6)(4, 5)$ , and  $(1, 6)(2, 5)(3, 8)(4, 7)$ , yielding  $\text{cov} [\mathcal{I}_1, \mathcal{I}_2] \text{cov} [\mathcal{I}_3, \mathcal{I}_4]$  and two other arrangements, and each of these three terms contribute the quantity

$$\gamma = \langle \mathcal{I}_b \rangle^4 \left[ \frac{\sqrt{\pi} \epsilon_0^4 \mathcal{T} \tau}{16} e^{-n^2 \tau^2 (\omega - 2\Omega)^2 / 4} + \sqrt{\pi} \mathcal{T} \tau e^{-n^2 \tau^2 \omega^2 / 4} \right]^2 \quad (\text{B10})$$

to the integral of ((B7)).

Finally, when the last term of ((B7)), whose value is given by squaring the right side of ((53)), is subtracted from the quantity  $\alpha + 6\beta + 3\gamma$  which is the sum of all the contributions the various contractions of  $\langle V_1 V_2 V_3 V_4 V_5 V_6 V_7 V_8 \rangle$  made to the integral of ((B7)), the variance of the power spectrum emerges as

$$\begin{aligned} \text{var}(|\tilde{\mathcal{I}}(\omega)|^2) = & \langle \mathcal{I}_b \rangle^4 \frac{\pi^2 \epsilon_0^4}{4} \delta^2(\omega - 2\Omega) \left[ \frac{\sqrt{\pi} \epsilon_0^4 \mathcal{T} \tau}{16} e^{-n^2 \tau^2 (\omega - 2\Omega)^2 / 4} + \sqrt{\pi} \mathcal{T} \tau e^{-n^2 \tau^2 \omega^2 / 4} \right] \\ & + 2 \langle \mathcal{I}_b \rangle^4 \left[ \frac{\sqrt{\pi} \epsilon_0^4 \mathcal{T} \tau}{16} e^{-n^2 \tau^2 (\omega - 2\Omega)^2 / 4} + \sqrt{\pi} \mathcal{T} \tau e^{-n^2 \tau^2 \omega^2 / 4} \right]^2. \end{aligned} \quad (\text{B11})$$

In the absence of the periodic signal, *i.e.* when  $\epsilon_0 = 0$ , the variance reduces to

$$\text{var}(|\tilde{\mathcal{I}}(\omega)|^2) = 2\pi \langle \mathcal{I}_b \rangle^4 \mathcal{T}^2 \tau^2 e^{-n^2 \tau^2 \omega^2 / 2}, \quad (\text{B12})$$

which is exponentially small at the frequency of the signal  $\omega = 2\Omega$  if  $\Omega > 1/(n\tau)$ , an inequality most easily satisfied when  $n$  (the number of orthonormal filters being employed to compute  $\mathcal{I}$ ) is large. In other words, when many filters are used the fluctuation in the background is negligibly small (and we have already shown in the main text that the mean background itself is also small).

To calculate the error in the signal itself, *once it is established by the above analysis to be many standard deviations above background*, one notes that the variance of the signal is dominated by the first term of ((B12)) while the signal itself by the first term of ((53)). Thus the ratio of the signal power to the standard deviation (standard error) in the power, or the first term of ((53)) divided by the square root of the first term of ((B12)), is of order  $\mathcal{T}/\tau \gg 1$ , and is independent of  $n$ .